AN EXPERIMENTAL INVESTIGATION

OF THE

BUNEMAN INSTABILITY

A Thesis

Submitted to the Faculty of Graduate Studies

in Partial Fulfillment of the Requirements

for the Degree of

MASTER OF SCIENCE

in the Department of Physics

University of Saskatchewan

by

JAMES DANIEL PAULSON

Saskatoon, Saskatchewan

April, 1981

ABSTRACT

The Plasma Betatron, a toroidal turbulent heating device, is modified so that a short (200 nsec duration) electric field pulse (maximum strength 650 V/m) is applied to accelerate electrons to a drift velocity V_D much larger than the initial thermal velocity V_{TH}. The device has a major radius of 19 cm and a minor radius of 3 cm, and a plasma having an electron density of $4 \times 10^{16} \sim 1.2 \times 10^{17}$ m^{-3} is prepared by rf ionization in a toroidal magnetic field of ~.2 T. A ratio of $V_D/V_{TH} \gtrsim 5$ has been realized which is sufficient for the development of the electron-ion two stream instability. Rapid decay of the plasma current, concurrent turbulent electron heating and an anomalously high electron-ion collision frequency are also observed. However, the Buneman frequency is not observed. Following the collapse of the current, strong oscillations near the ion plasma frequency are detected. Most of the experimental results are in qualitative agreement with recent theoretical predictions.

ACKNOWLEDGEMENTS

The author would like to express his appreciation to all those people who have assisted him in the completion of this work. In particular, Dr. A. Hirose whose assistance and supervision made this thesis possible. Dr. H.M. Skarsgard provided much appreciated observations and criticisms. Important discussion regarding the nonlinear theory of the instability was received from Dr. O. Ishihara. Valuable technical assistance came from J. Ratzlaff and A. Witmans. Special thanks go to V. Cyr who typed this thesis. Finally, I would like to acknowledge the support and patience of my wife Kim, throughout the long preparation of this work.

This research was supported by grants from the Natural Sciences and Engineering Research Council of Canada.

TABLE OF CONTENTS

TABLE OF CONTENTS (Cont.)

LIST OF FIGURES

LIST OF FIGURES (Cont.)

LIST OF FIGURES (Cont.)

CHAPTER 1

INTRODUCTION

If the electrons in a plasma are accelerated by an electric field to a velocity much greater than their average thermal velocity within one characteristic electron-ion collision time, they can be expected to accelerate freely without limit. Dreicer (1959) determined the critical field strength E_c necessary to accomplish this phenomenon to be approximately

$$E_c = 3 \times 10^{-16} \frac{n}{T_e} \quad (V/m) \tag{1.1}$$

where n is the electron density (m^{-3}) and T_e is the electron temperature (eV). As an example, consider a plasma having $n = 5 \times 10^{16}$ m^{-3} and $T_e = 7$ eV. These values correspond to the initial plasma parameters in the Plasma Betatron. The runaway field required in this case is only 2 V/m. This field strength is easily obtained experimentally. In spite of this most attempts to create free acceleration for an extended period of time have failed except for extremely low plasma densities (Skarsgard 1958). In toroidal devices, such as the Plasma Betatron, free acceleration of electrons has been achieved only for very short times immediately following the application of the electric field pulse (Skarsgard and Strilchuk 1965; Stefanovsky 1965). The electron drift velocity in the Plasma Betatron has never exceeded the thermal velocity by a factor of more than 2.

The observed departure from free acceleration can be attributed to the onset of plasma instabilities. It is well known that a

current flow in a plasma (i.e. a relative drift between the electrons and ions) can excite instabilities. The electron-ion two stream (Budker 1956; Buneman 1959), the trapped particle (Hirose et al. 1972) and the ion acoustic (E.A. Jackson 1960) instabilities are examples of this class of instability. The uniformity of the toroidal magnetic field in the Plasma Betatron is relatively poor or the magnetic field is "bumpy". It has been shown (Whitfield and Skarsgard 1974) that this nonuniformity can enhance the effective electron collision frequency. The conventional Buneman and ion acoustic instabilities enhance the effective collision frequency as a result of ion density perturbations caused by the instabilities themselves.

The Budker-Buneman instability has been considered to pose the greatest threat to achieving free acceleration, but at the same time to be the most effective in turbulent heating. In order to heat a plasma efficiently by passing a current through it the resistivity of the plasma must not, as is expected classically, decrease with temperature. The rapid onset of the violent Buneman instability can bring about a high anomalous resistivity thus making turbulent heating a practical method for plasma heating. The major requirement for the instability to occur is that the electron drift velocity V_D be much greater than the electron thermal velocity V_{TH}. As is explained in Chapter 2, if this condition is not met the hydrodynamic Buneman instability cannot exist and the kinetic ion acoustic instability will dominate (Tanaca et al. 1967). As stated above, achieving a period of free acceleration long enough to boost the electron drift velocity to

meet this condition is difficult, and there has not been a clear cut experimental verification of the instability. Hamberger and Jancarik (1972) reported that they observed electrostatic oscillations at the frequency predicted by Buneman and consequent anomalous resistivity. However, it is not obvious that the condition, $V_D >> V_{TH}$, was satisfied in their experiment as no time resolved electron temperature measurements were performed. Moreover, as shown in Chapter 2 it should be practically impossible to observe the so-called Buneman frequency since the linear stage of the instability is extremely short-lived. Iizuka et al. (1979) have also claimed that they have observed the Buneman instability. In their experiment, however, not all of the electrons are drifting relative to the ions so it is inappropriate to call the observed instability Buneman. Furthermore, their experiment cannot be treated as an initial value problem, as in their theory, because of the existence of boundary conditions.

The principle aims of the present work are

a) to create the experimental condition $V_D >> V_{TH}$ for the Budker-Buneman instability, and

b) to study the behaviour of a plasma after this condition has been established.

A basic method which could be used to overcome the thermal velocity barrier was pointed out by Hirose and Alexeff (1974). If the electron collision frequency

$$\frac{1}{V_D} \frac{d V_D}{dt}$$

where V_D is the electron drift velocity and dV_D/dt is the electron drift acceleration, is larger than the typical growth rate of the instability the electron drift velocity will be varying too rapidly for the instability, which requires an adiabatic system, to grow. The applied electric field pulse must be fast rising in order to produce this rapid acceleration. The pulse should also be of short duration to avoid additional energy input after the instability begins to grow. This last condition will simplify the theoretical analysis of the experiment.

The investigation to be presented in this thesis was carried out using the Plasma Betatron. This is a toroidal device which, as mentioned previously, has exhibited the brief period of free acceleration followed by electron heating. Figure 1.1 shows the shape of a typical electric field pulse previously produced by the machine. Figure 1.2 illustrates the electron drift, thermal and expected free acceleration velocities for the pulse shown. Note that the electron drift velocity exceeds the electron thermal velocity by at most a factor of 2, and then only for a very short time (~80 nsec). We modified the Plasma Betatron to produce a much shorter and more importantly, a faster rising electric field pulse. We used the brief period of free acceleration to boost the electron drift velocity to a value much greater than the electron thermal velocity. In this way we were able to satisfy the most important requirement for the Buneman instability.

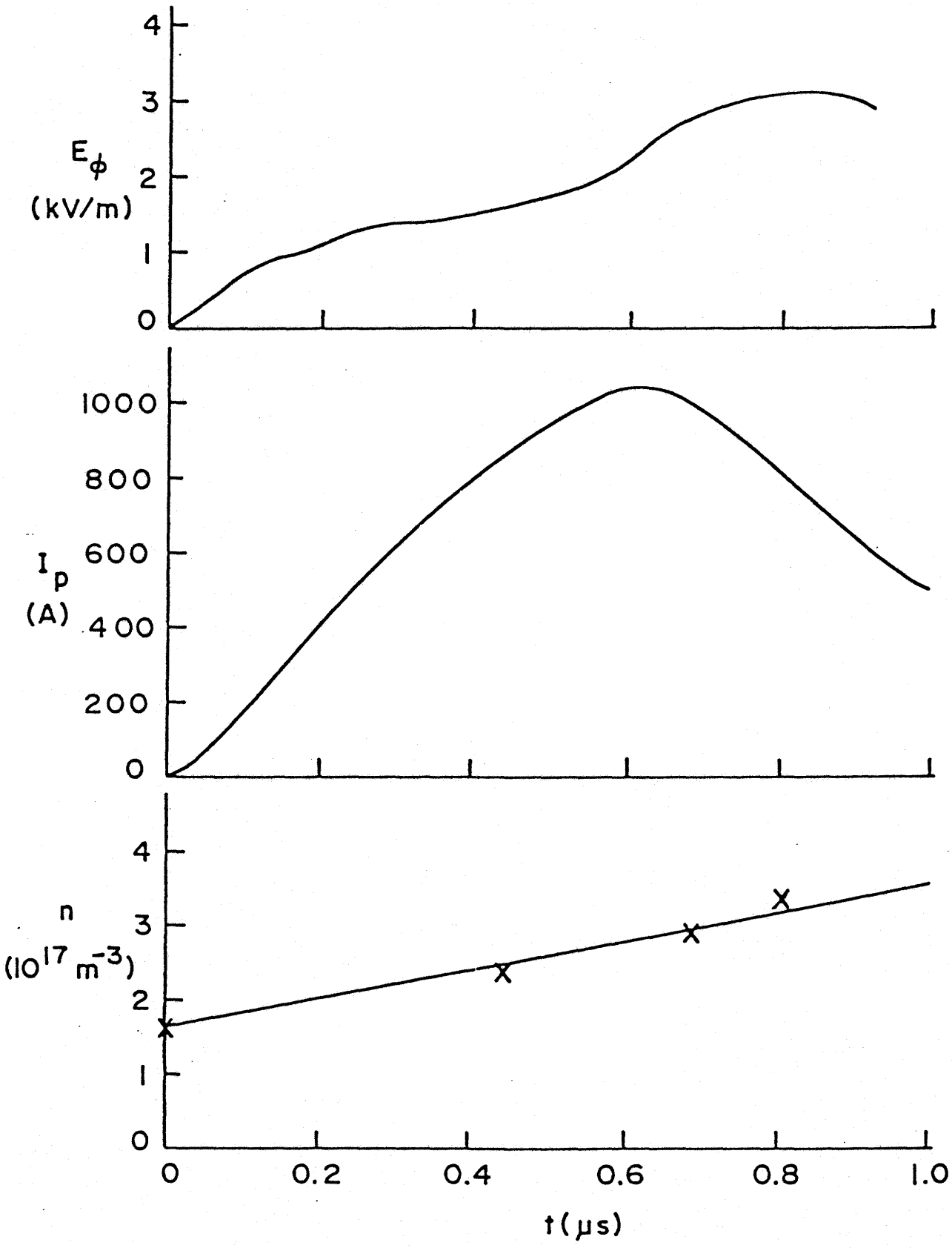

Fig. 1.1 Electric field E_ϕ, plasma current I_p and average electron density n in the Plasma Betatron before modification for the present investigation.

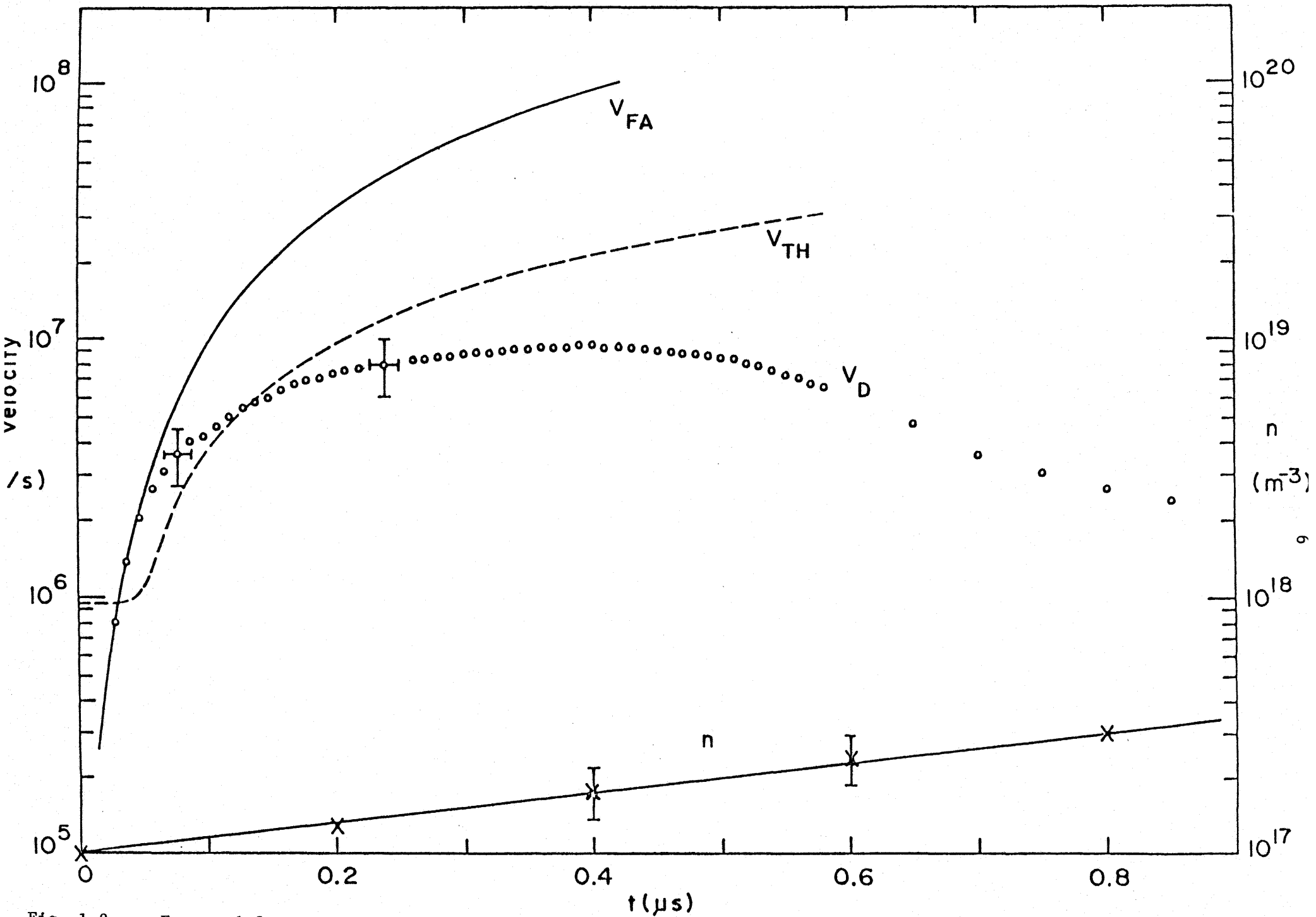

Fig. 1.2. Expected free acceleration velocity V_{FA}, thermal velocity V_{TH} and electron drift velocity V_D in the Plasma Betatron before modification for the present investigation

Chapter 2 will provide a brief overview of the theory relevant to the Buneman instability in toroidal machines. This chapter deals with the linear theory and discusses some of the nonlinear aspects of the Buneman instability.

Chapter 3 will describe the modifications made to the Plasma Betatron. It will also give a brief description of the machine in general and the diagnostics used in this investigation.

Experimental results will be presented in Chapter 4. The drift velocity of the electrons is shown to exceed their thermal velocity by a factor of at least 5. The decay times of the plasma current are considered. The effective electron collision frequency is calculated. The results of electrostatic probe measurements are presented. Finally, a comparison of the experimental results is made with predictions from the recent nonlinear theory of Ishihara, Hirose and Langdon (1980).

Chapter 5 contains a summary of the experimental work and a conclusion.

The MKS system of units is used throughout this thesis unless otherwise specified.

CHAPTER 2

THEORETICAL BACKGROUND

2.1 Review of linear theory

The Buneman instability is a nonresonant (hydrodynamic) instability which is expected to occur only if the electron drift velocity far exceeds the electron thermal velocity. It is one of the two stream instabilities caused by the interaction between a cold electron beam and stationary cold ions. The instability is nonresonant in that both the ion and electron particle velocities are far removed from the phase velocity of the wave. This prevents any resonant particle-wave interaction as, for example, in the ion acoustic instability.

The linear theory of the Buneman instability has been developed by Buneman (1959), E.A. Jackson (1960), and J.D. Jackson (1960). In particular, J.D. Jackson showed that if the electron drift velocity exceeds the thermal velocity by a factor of 6, the cold plasma approximation used in the derivation contained in Appendix A, as well as in the recent nonlinear theory described later, is valid. For lower drift velocities a smooth transition to the ion acoustic instability, which has a smaller growth rate than the Buneman instability, occurs. Figure 2.1 illustrates the similarity between the ion acoustic and the Buneman instabilities.

As will be discussed in the following section, the period of linear growth for the Buneman instability lasts for only a few growth

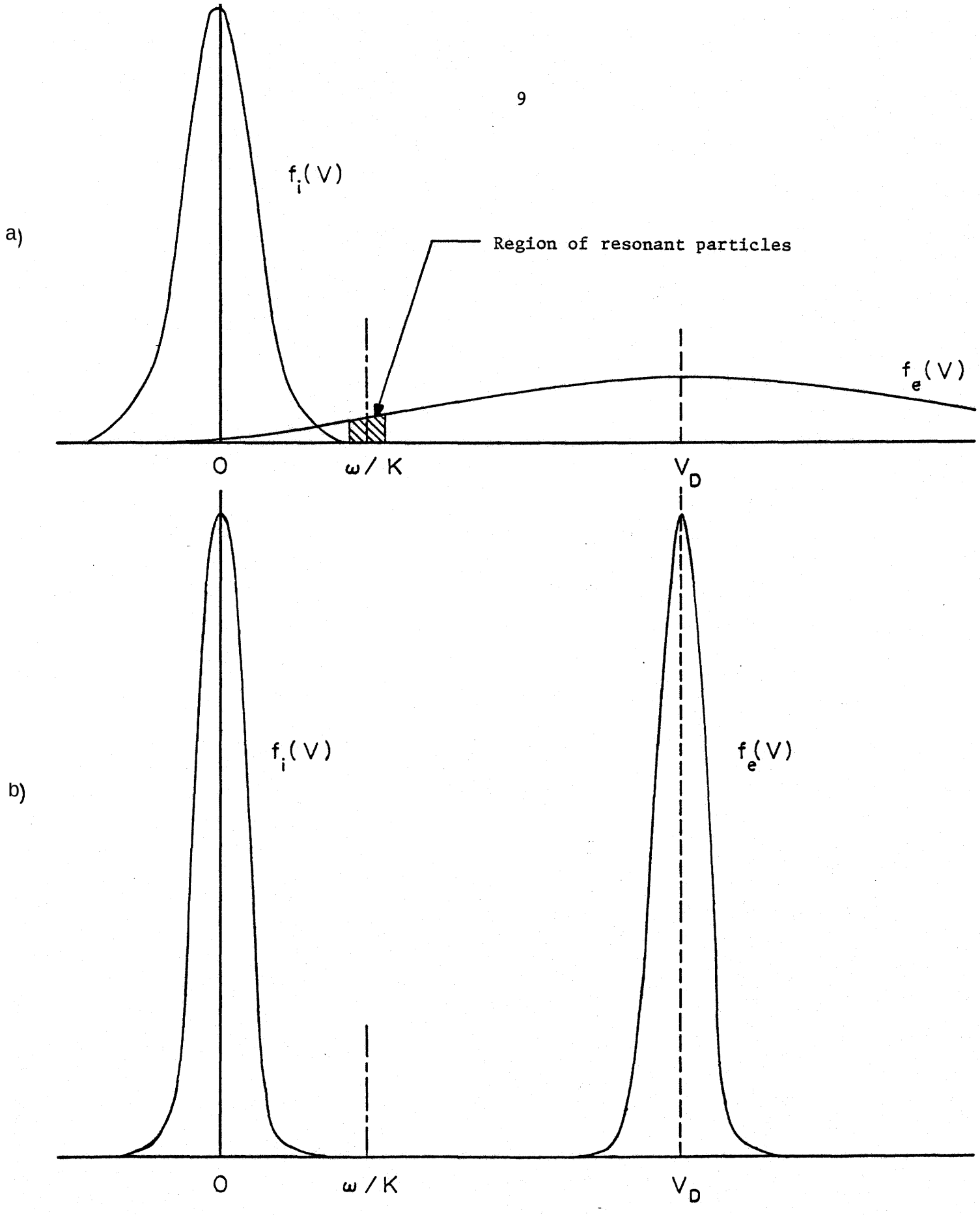

Fig. 2.1. Electron $f_e(V)$ and ion $f_i(V)$ velocity distributions for the cases of
(a) ion acoustic instability and
(b) Buneman instability.
V_D is the drift velocity of the electrons relative to the ions
ω/K is the phase velocity of the wave.

times. The instability quickly enters a nonlinear stage. This fact makes it practically impossible to detect the frequency of the instability. Despite its short period of validity, the linear theory does show us a mechanism for the instability and illustrates the plasma conditions which must be met in order for the instability to occur.

As shown in Appendix A, the linear dispersion relation for electrostatic waves in a plasma which is composed of cold drifting electrons and stationary cold ions is given by

$$1 = \frac{\omega_{pe}^2}{(\omega - KV_D)^2} + \frac{\omega_{pi}^2}{\omega^2} \tag{2.1}$$

where ω_{pe} and ω_{pi} are the electron and ion plasma frequencies, ω and K are the frequency and wavenumber of the wave and V_D is the electron drift velocity. The above dispersion relation is subject to several major constraints. First, the drift velocity must be a constant otherwise the dispersion relation must be replaced by the proper differential equation. Second, the wave must be one dimensional, propagating only along the direction of the drift velocity V_D. In the Plasma Betatron, used for the experimental studies described later, a toroidal magnetic field is always present to confine the plasma. If the waves are allowed to propagate at an angle θ to the drift velocity, which is along the magnetic field, the dispersion relation given above should be modified as

$$1 + \frac{\omega_{pe}^2}{\Omega_e^2} \sin^2\theta = \frac{\omega_{pe}^2 \cos^2\theta}{(\omega - K_{\parallel}V_D)} + \frac{\omega_{pi}^2}{\omega^2} \tag{2.2}$$

where $K_{\parallel} = K\cos\theta$ and Ω_e is the electron cyclotron frequency. As shown in Appendix A, the growth rate is a maximum for $\theta = 0$. Therefore, even if there are unstable modes obliquely propagating, the plasma dynamics are expected to be dominated by the fastest growing mode, and the one dimensionality assumed should not cause too large an error. Third, it is assumed that the plasma is boundary free, or that the dispersion relation is a local dispersion relation. Since the Plasma Betatron is a toroidal device there is no boundary in the direction of the electron drift velocity. However, the plasma is radially limited (the minor plasma radius $\simeq$ 2.5 cm) and for the assumption to be valid the wavelength along the drift velocity should be much shorter than the plasma radius. As will be shown later (Section 4.2.4), this condition is well satisfied for the plasma parameters used.

Equation 2.1 is a fourth order algebraic equation for ω with a given real wavenumber K and can be easily solved numerically. The case for an Argon plasma is shown in Fig. 2.2. The growth rate is sharply peaked at the resonance $kV_D \simeq \omega_{pe}$. The frequency and growth rate at the peak are given approximately by

$$\omega_o = \frac{1}{2}\left(\frac{m}{2M}\right)^{1/3}\left[1 + \frac{1}{2}\left(\frac{m}{2M}\right)^{1/3}\right]\omega_{pe}$$

$$\gamma_o = \frac{\sqrt{3}}{2}\left(\frac{m}{2M}\right)^{1/3}\left[1 - \frac{1}{2}\left(\frac{m}{2M}\right)^{1/3}\right]\omega_{pe} \qquad (2.3)$$

where m/M is the electron to ion mass ratio (M/m = 40 × 1836 for a singly ionized argon plasma). For the range $KV_D << \omega_{pe}$, Eq. 2.2

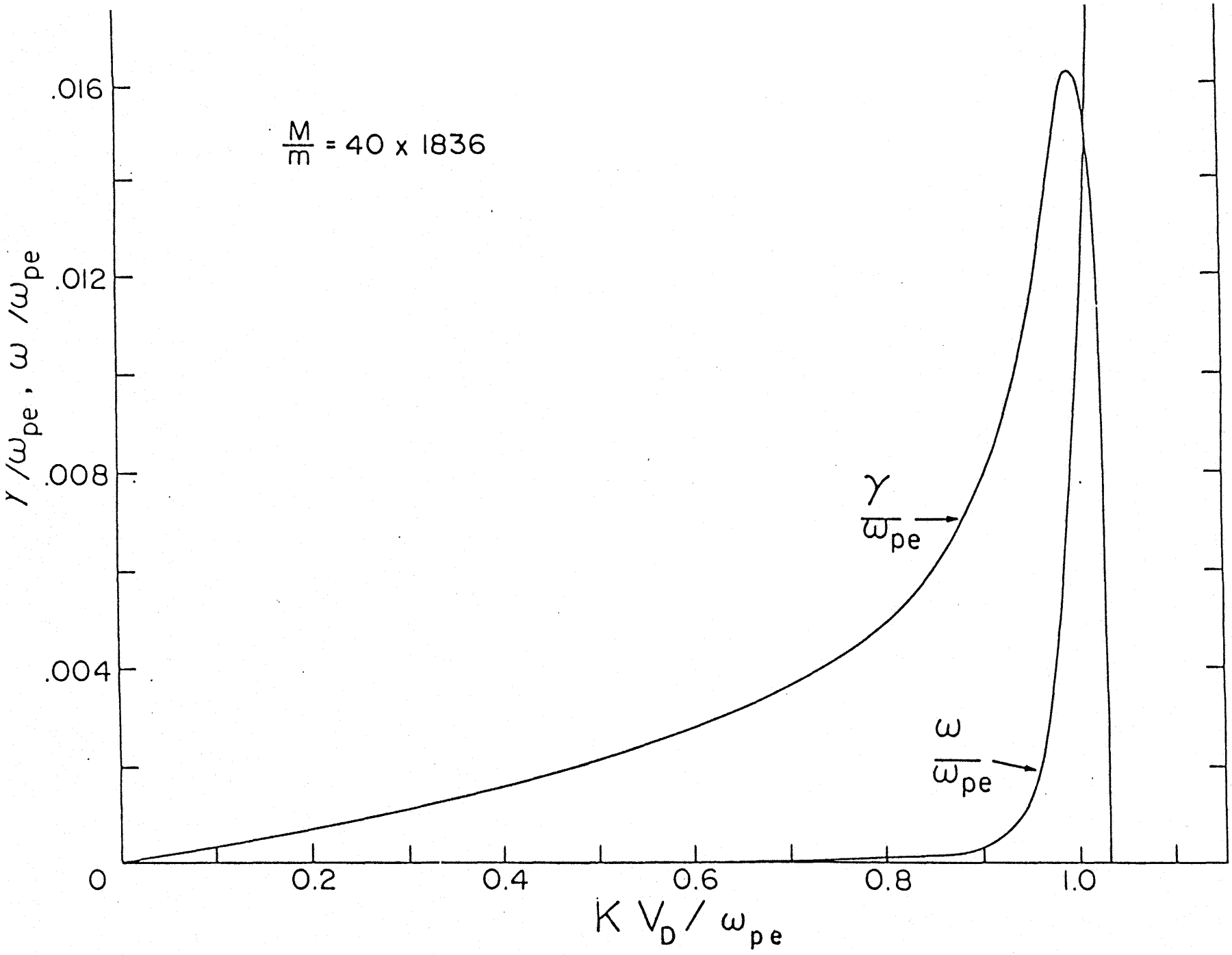

Fig. 2.2. Normalized growth rate γ and real frequency ω for the Buneman instability according to linear theory.

yields

$$\gamma(K) \simeq \sqrt{m/M}\, KV_D \ , \quad \omega \simeq 0 \quad . \tag{2.4}$$

In view of the sharp resonance in the growth rate profile the mode $K \simeq \omega_{pe}/V_D$ will have the dominant influence in the evolution of the Buneman instability, as shown in Appendix B, provided there is sufficient time before the instability saturates.

The resonance mode has a large growth rate, $\gamma_o > \omega_o$, and the instability is almost aperiodic. In one oscillation period the mode would e-fold $2\sqrt{3}\ \pi \simeq 11$ times. This means the amplitude of perturbed quantities such as electric field and the plasma density perturbation would increase by a factor of 5.3×10^4, and the fluctuation energy, which is proportional to the square of the perturbed quantities, by a factor of 2.8×10^9. A quiescent plasma can be characterized by its intrinsic thermal fluctuation level. The ratio between the electric field fluctuation energy and the plasma thermal energy is of the order of the plasma parameter $(n\lambda_D^3)^{-1}$ (Ichimaru 1973), where n is the electron density and λ_D is the Debye length,

$$\lambda_D = \sqrt{\varepsilon_o T_e / ne^2} \quad .$$

Here ε_o is the permittivity of free space, T_e is the electron thermal energy (in Joules) and e is the charge on the electron. For typical Plasma Betatron parameters, $n = 10^{17}\ m^{-3}$, $T_e = 10$ eV the thermal fluctuation level is of the order of 10^{-5}. The nonthermal electron kinetic energy produced in the Plasma Betatron is at most 50 T_e. Therefore, the

maximum possible fluctuation energy amplification possible is about 5×10^6, which is far below the amplification expected during one oscillation period. In other words, we have to conclude that it is practically impossible to experimentally observe the frequency, ω_o, as the linear stage of the instability will terminate well before the end of the first oscillation period.

2.2 Nonlinear aspects of the Buneman instability

Buneman (1959) carried out a computer simulation on the electron-ion two stream instability using relatively few electron-ion pairs. Rapid thermalization of the electron drift energy caused by trapping was demonstrated.

Recently, Hirose (1978) and Ishihara, Hirose and Langdon (1980) have developed analytical models to describe the nonlinear stage of the instability. The nonlinear dispersion relation derived by them can predict the breakdown of the linear growth stage and the final saturation level of the wave energy. These results have been verified by computer simulation. The results of the nonlinear theory are summarized here as later experimental results will be compared directly with these theoretical predictions.

As pointed out in the previous section, the Buneman instability is almost aperiodic and it is not obvious that the conventional quasilinear theory (Drummond and Pines 1962; Vedenov, Velikhov and Sagdeev 1962) can be applied to such a "strong" instability. Bartlett (1968) made an attempt to generalize the theory to the case $\gamma_o \gtrsim \omega_o$.

His theory can describe the breakdown of the linear growth stage but does not demonstrate saturation of the instability. The theory developed by Ishihara, Hirose and Langdon has shown that the quasilinear theory is still applicable provided the frequency shift is properly taken into account. In the conventional quasilinear theory, only the growth rate is allowed to vary. The theory developed by Ishihara et al. may be appropriately called a generalized quasilinear theory.

In addition to the quasilinear effects, which decelerate and heat the electrons, it has been shown, by Ishihara et al., that nonlinear mode coupling must be included to describe the nonlinear stage of the instability. As the amplitude of the fastest growing mode increases, higher harmonics are generated which in turn affect the fundamental mode. Only if this mode coupling is included will the analytical model yield a saturation level consistent with that found by computer simulation.

In Fig. 2.3, the evolution of the electrostatic energy normalized by the initial electron drift energy is shown for three models, the linear model and the generalized quasilinear model with and without mode coupling. The departure from the linear growth stage occurs at a relatively small field energy consistent with a model derived by Hirose (1978). The result of the recent computer simulation is also shown in Fig. 2.3. It is evident that the generalized quasilinear theory is in excellent agreement with the simulation.

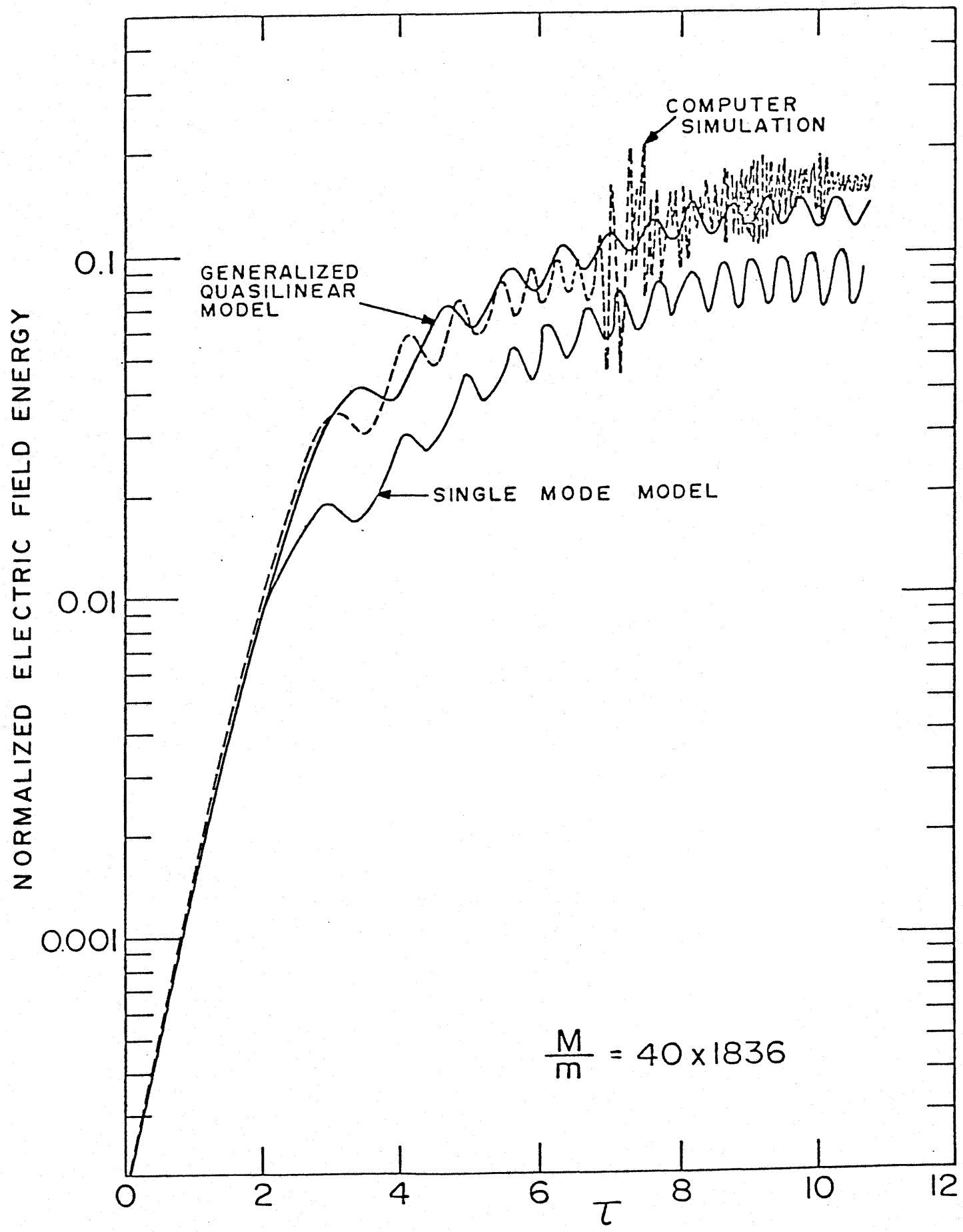

Fig. 2.3. Normalized electrostatic field energy as a function of $T = \gamma_o t$ where γ_o is the maximum linear growth rate and t is time.

Plasma parameters which can be observed in the Plasma Betatron include the electron temperature, average electron density, the electron drift velocity and fluctuating electric fields (see Chapter 3).

Figure 2.4 shows the collapse of the electron beam as predicted by Ishihara et al. (1980). The electrons are completely thermalized after only 7-8 growth periods. The electron drift energy is entirely converted into thermal and wave energy. In the experiment, this should appear as a sudden collapse of the plasma current.

The theory also predicts an ion sloshing motion near $2\omega_{pi}$, where ω_{pi} is the ion plasma frequency. This should be observed after the breakdown of the plasma current.

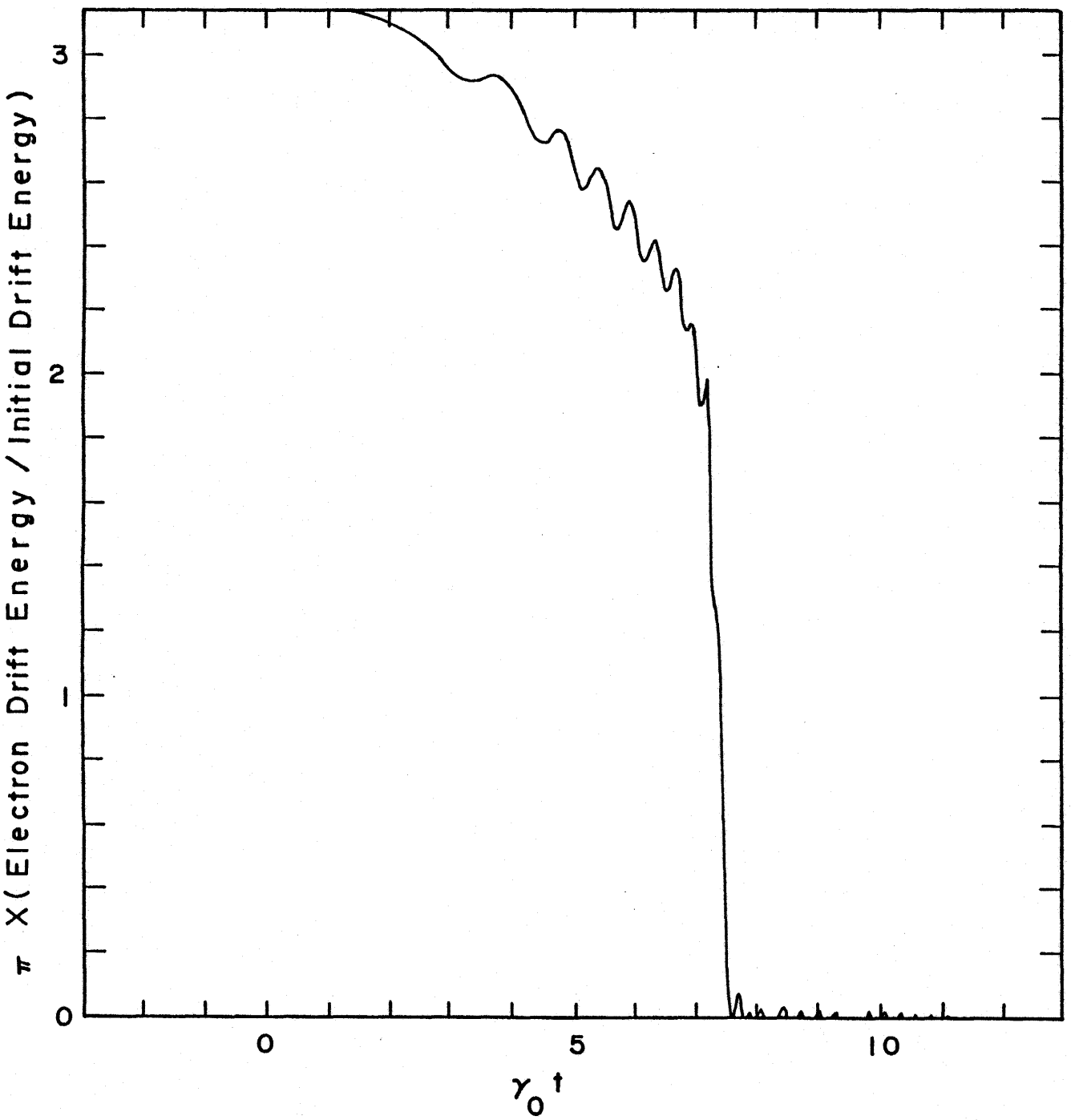

Fig. 2.4. Electron drift energy as predicted by computer simulation.

CHAPTER 3

THE EXPERIMENTAL SYSTEM AND DIAGNOSTICS

3.1 The Plasma Betatron

The physical aspects of the Plasma Betatron located at the University of Saskatchewan have been described in detail previously (Gore 1961; Skarsgard and Gore 1965). This chapter will give only a brief description of the device and describe the modifications pertaining to this experiment.

The vacuum chamber, shown in Fig. 3.1, is a Pyrex torus with a major radius of 19 cm and a minor radius of 3 cm. There are six symmetrically located ports to allow for pumping, gas inlet and diagnostics.

The vessel is evacuated by means of a mercury diffusion pump to a base pressure of about 1×10^{-6} Torr. A steady flow of gas, argon in this experiment, at the desired pressure is then set up by adjusting the gas inlet needle valve. The gas pressure is measured with an ionization gauge.

The toroidal magnetic field B_ϕ is provided by 18 coils symmetrically placed around the chamber. The maximum magnetic field obtainable is .4 T. For this experiment a field of about .2 T was used as it proved to be the best compromise between optimizing the orbit analyzer probe data and obtaining consistent preionization.

The plasma is produced by a radio frequency oscillator

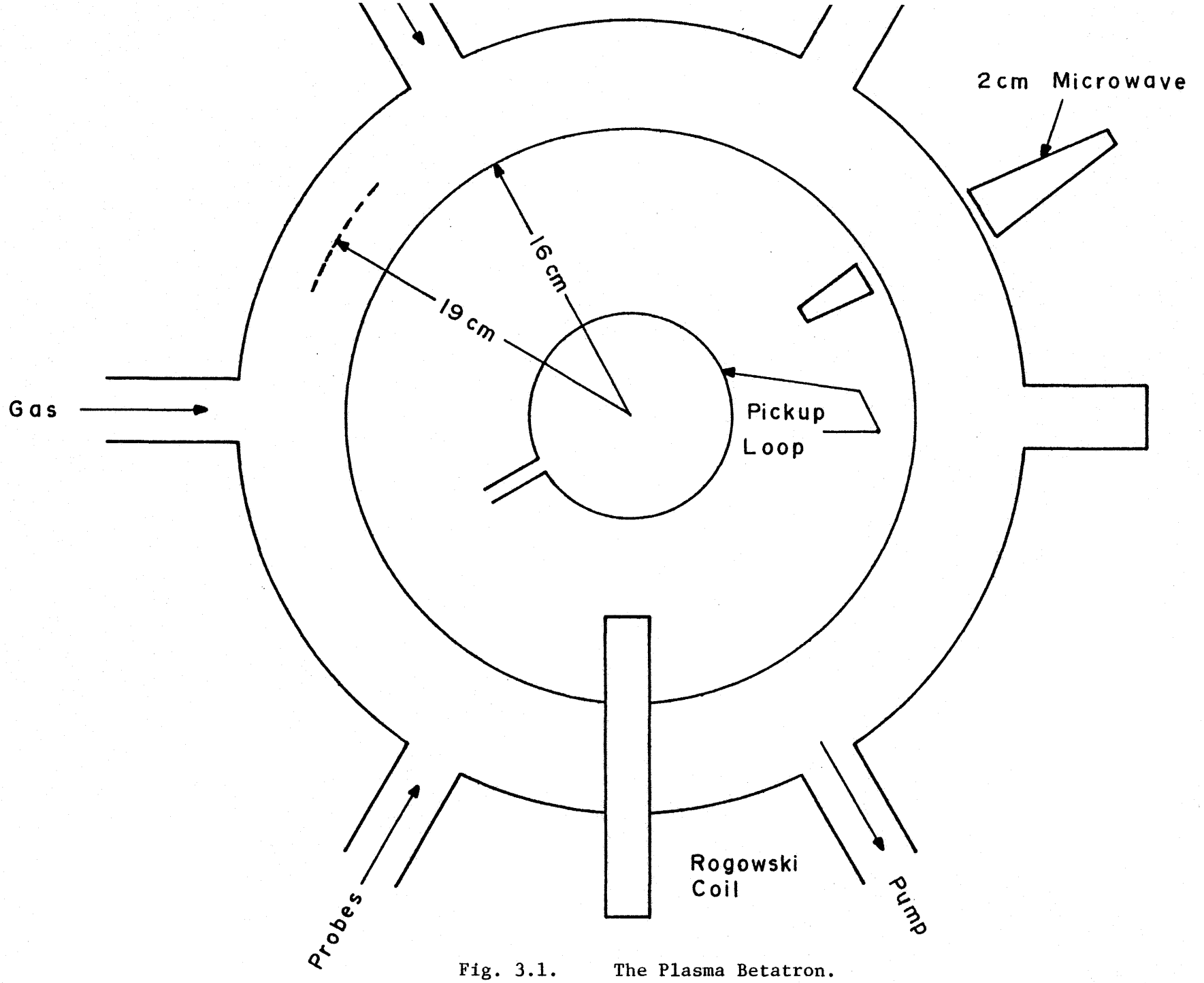

Fig. 3.1. The Plasma Betatron.

(~5 kW into a resistive load at 3 MHz) coupled inductively to the chamber. When used at the peak of the pulsed magnetic field and when the ionization gauge is on, the rf field can provide densities up to 1.2×10^{17} m^{-3} with a gas pressure of 5.6×10^{-4} Torr. The rf field decays with time. The plasma density depends upon the amplitude of the field so the density at the time the rf is switched off can be controlled by varying the rf duration.

The fast rising electric field pulse needed to accelerate the electrons was applied to the plasma through the toroidal electric field winding shown in Fig. 3.2. This winding consists of four specially placed turns which were previously used to produce a betatron type field configuration. Before modification the energy was provided by two 5 μF capacitor banks which were charged in parallel and then discharged in series by means of spark gap switches. For this experiment one capacitor bank was disconnected and the connections to the windings were shorted. The capacitors in the remaining bank were replaced with four .0075 μF discharge type capacitors in a series-parallel arrangement to give a total capacitance of .0075 μF. The schematic diagram of the modified circuit is given in Fig. 3.3. This change considerably reduced the stored energy but allowed the creation of the short pulse shown in Fig. 3.4. The circuit was crowbarred near the end of the first quarter cycle of the voltage across the windings. An electric field rise time of 20 nsec and a pulse width of 100 nsec were realized. The finite resistance of the crowbarring spark gap causes some voltage reversal in the pickup loop signal (Section 3.2.3).

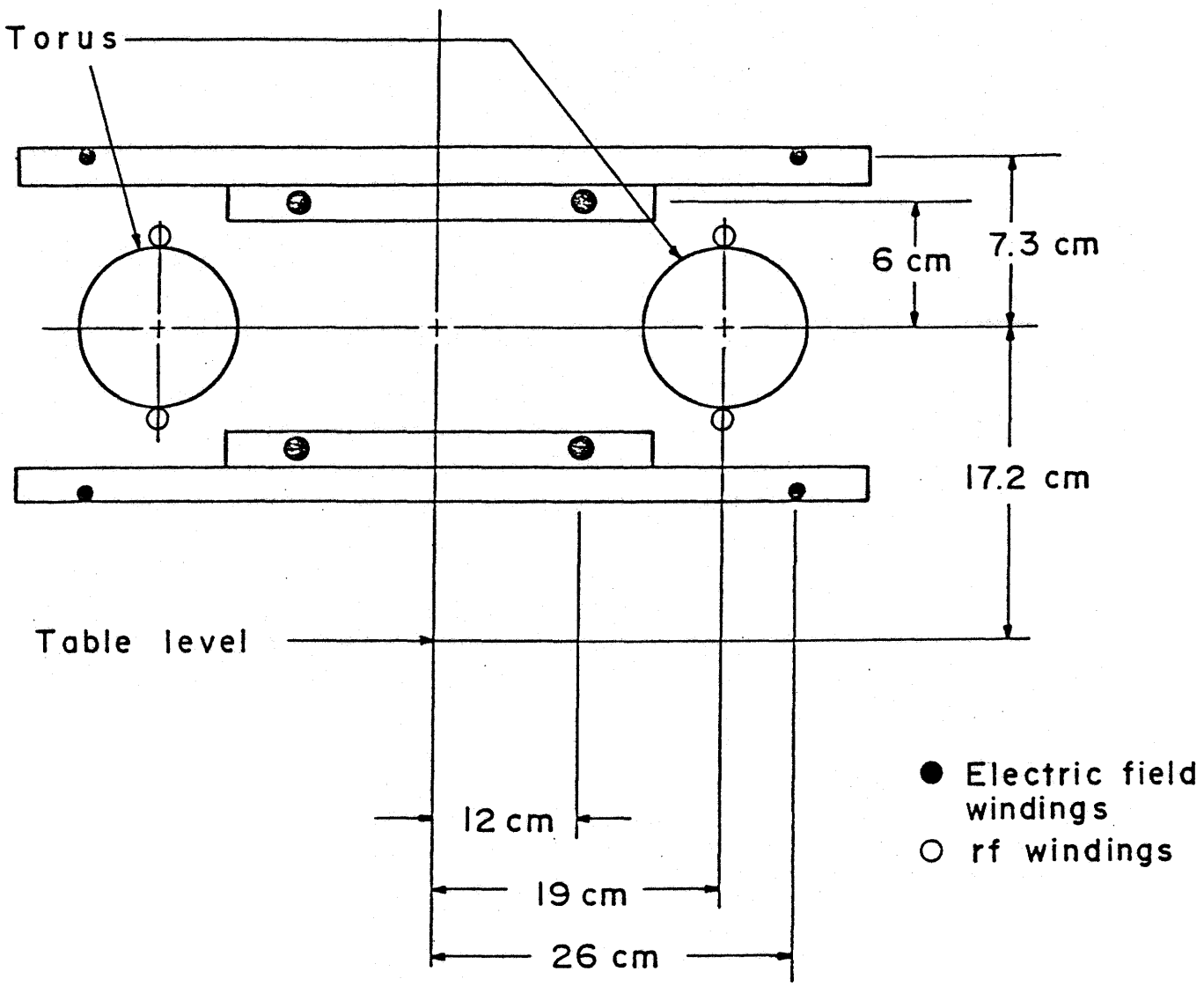

Fig. 3.2. Electric field winding locations in the Plasma Betatron

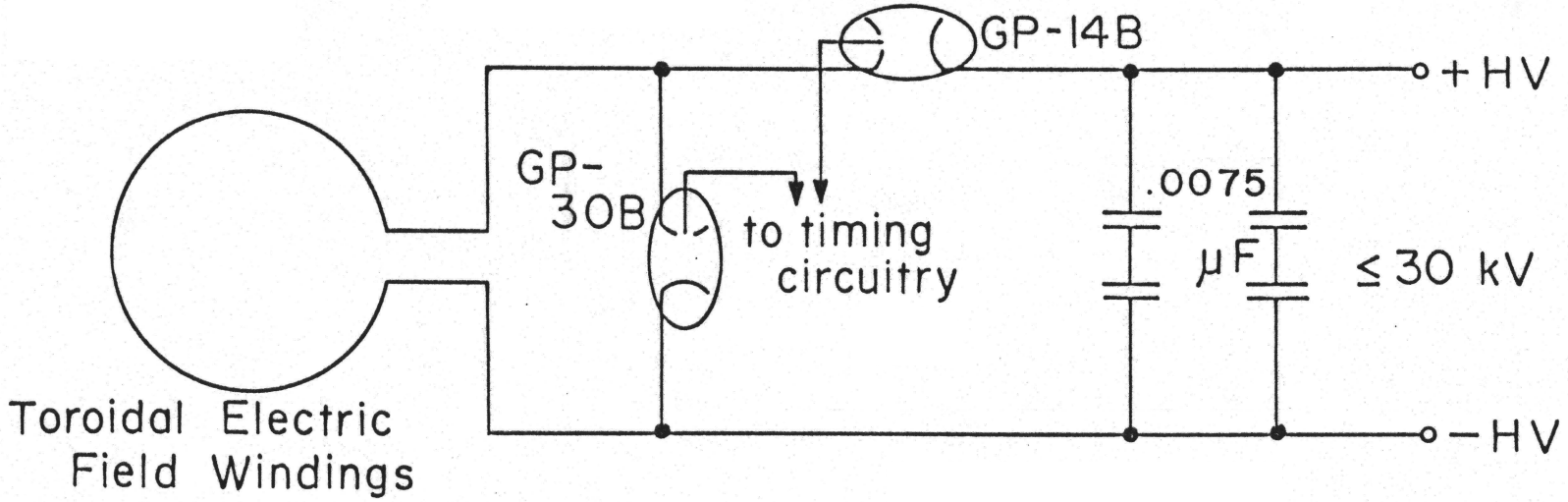

Fig. 3.3. Schematic diagram of the electric field pulse circuitry.

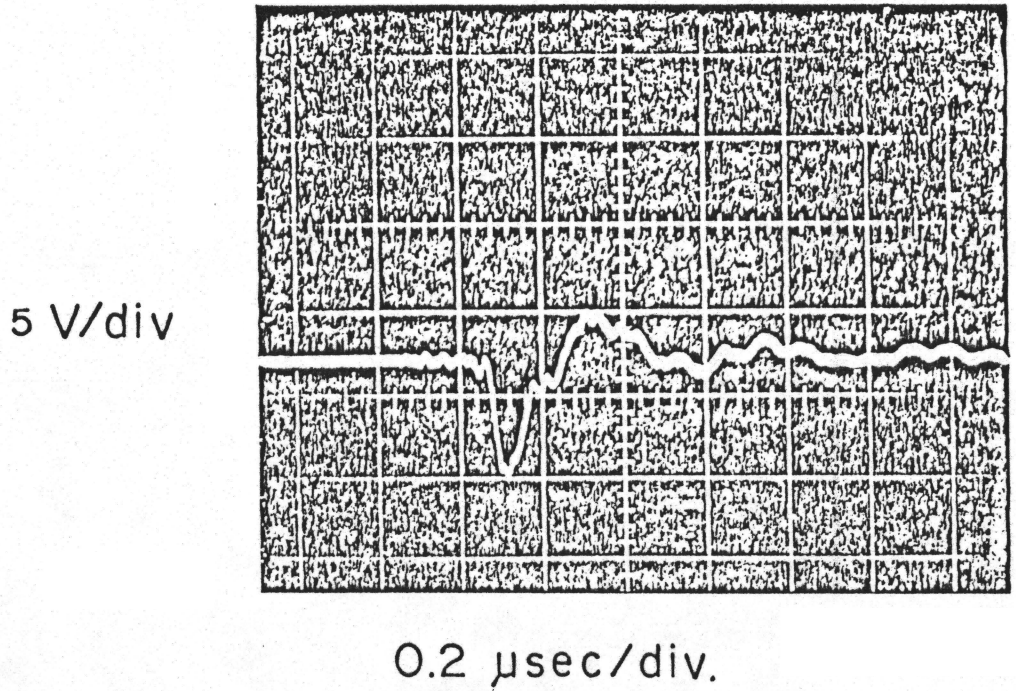

Fig. 3.4. Output of the pickup loop without plasma current showing the shape of the pulse produced by the circuit of Fig. 3.3.

The timing sequence for a single pulse with this apparatus is shown in Fig. 3.5. With the gas pressure adjusted to 5.6×10^{-4} Torr the toroidal magnetic field B_ϕ is applied. Following this the rf field is turned on at a time such that it can be terminated near the peak of the magnetic field waveform. The rf duration is such that the desired density exists when the toroidal electric field pulse is applied approximately 30 μsec after the end of the rf. This delay allows the density to drop from the large value necessary for consistent ionization as well as removing a source of electrical noise from the time frame of the experiment.

3.2 Diagnostics

3.2.1 Introduction

The following sections provide a brief description of the plasma diagnostics available on the Plasma Betatron. References containing a more complete discussion of each diagnostic are given.

The plasma current is monitored during and after the application of the electric field pulse by a Rogowski coil. The electric field itself is measured with a pickup loop. The initial plasma density is determined with a 17 GHz interferometer.

The initial electron temperature is measured using a double Langmuir probe. After the start of the electric field pulse the electron temperature is monitored with a charge selective orbit analyzer probe.

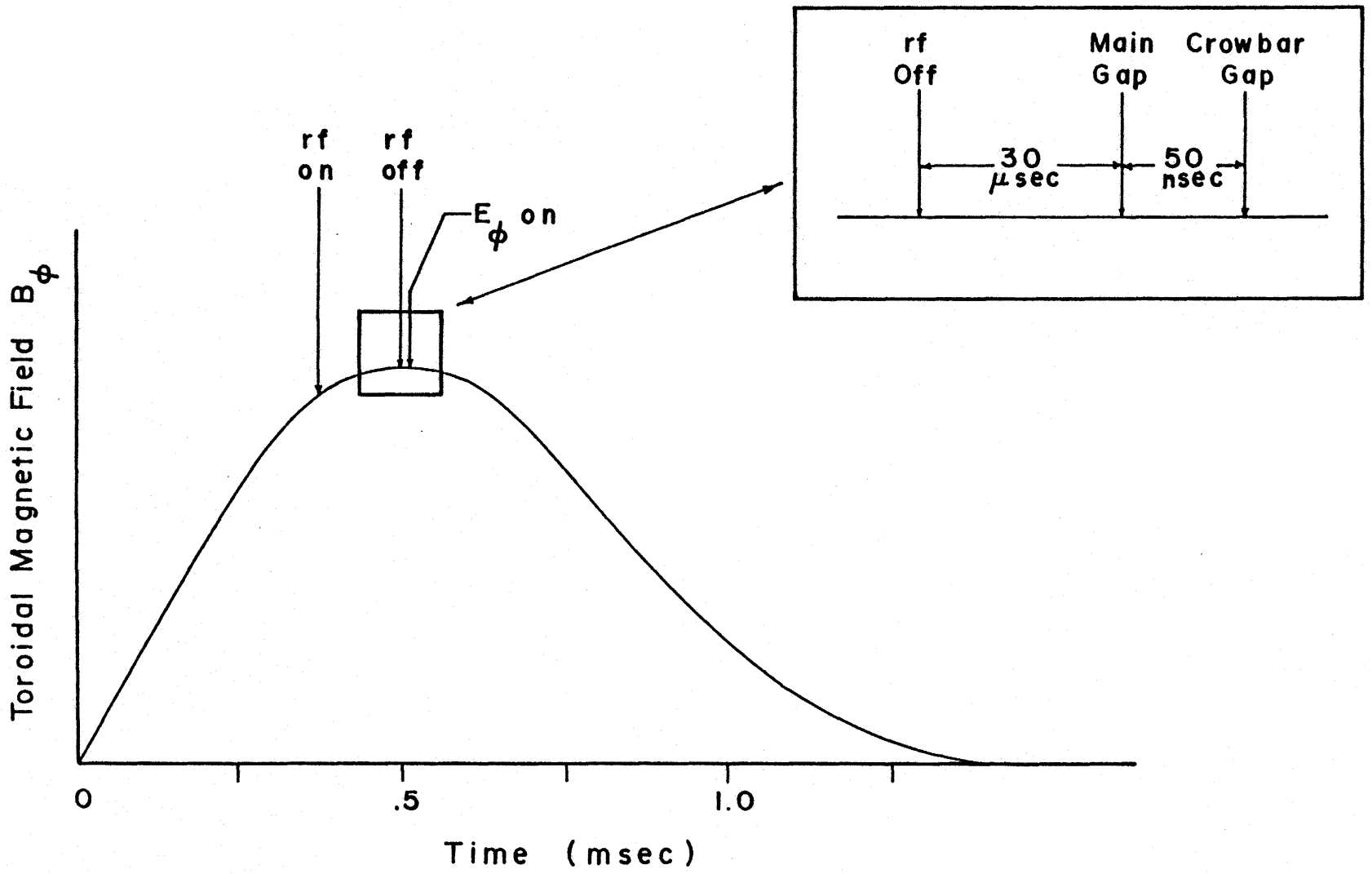

Fig. 3.5. Timing sequence for a typical discharge.

An unsuccessful attempt to observe ion fluctuations was made using a Spex 1702 spectrometer. Electrical noise levels proved to be too great to obtain usable data.

3.2.2 The Rogowski coil

A Rogowski coil is a toroidal coil placed around the plasma chamber. The coil used was counter-wound to provide a noise cancelling differential output. It was rectangular in cross-section and shielded against unwanted magnetic flux by a brass case. The electrical and mechanical properties of the coil are described by Strilchuk (1971). The frequency response of the coil is given in Fig. 3.6. The output of the coil was integrated electrically with a time constant of 18 μsec and corrected manually for a delay of 20 nsec. The sensitivity is 1250 ± 50 A/V.

3.2.3 The pickup loop

The pickup loop used is also described in detail by Strilchuk (1971). It is a single turn circular wire loop located 17 cm below and coaxial with the plasma chamber. The loop is terminated with an electrical network which gives it a uniform frequency response up to about 20 MHz as well as matching it to a 50 Ω cable and a 50 Ω load resistor. The equation used to determine the electric field E_ϕ within the torus from the loop output voltage V_o is

$$E_\phi = 197\ V_o - 3.24 \times 10^{-7} \frac{di_p}{dt} \qquad (3.1)$$

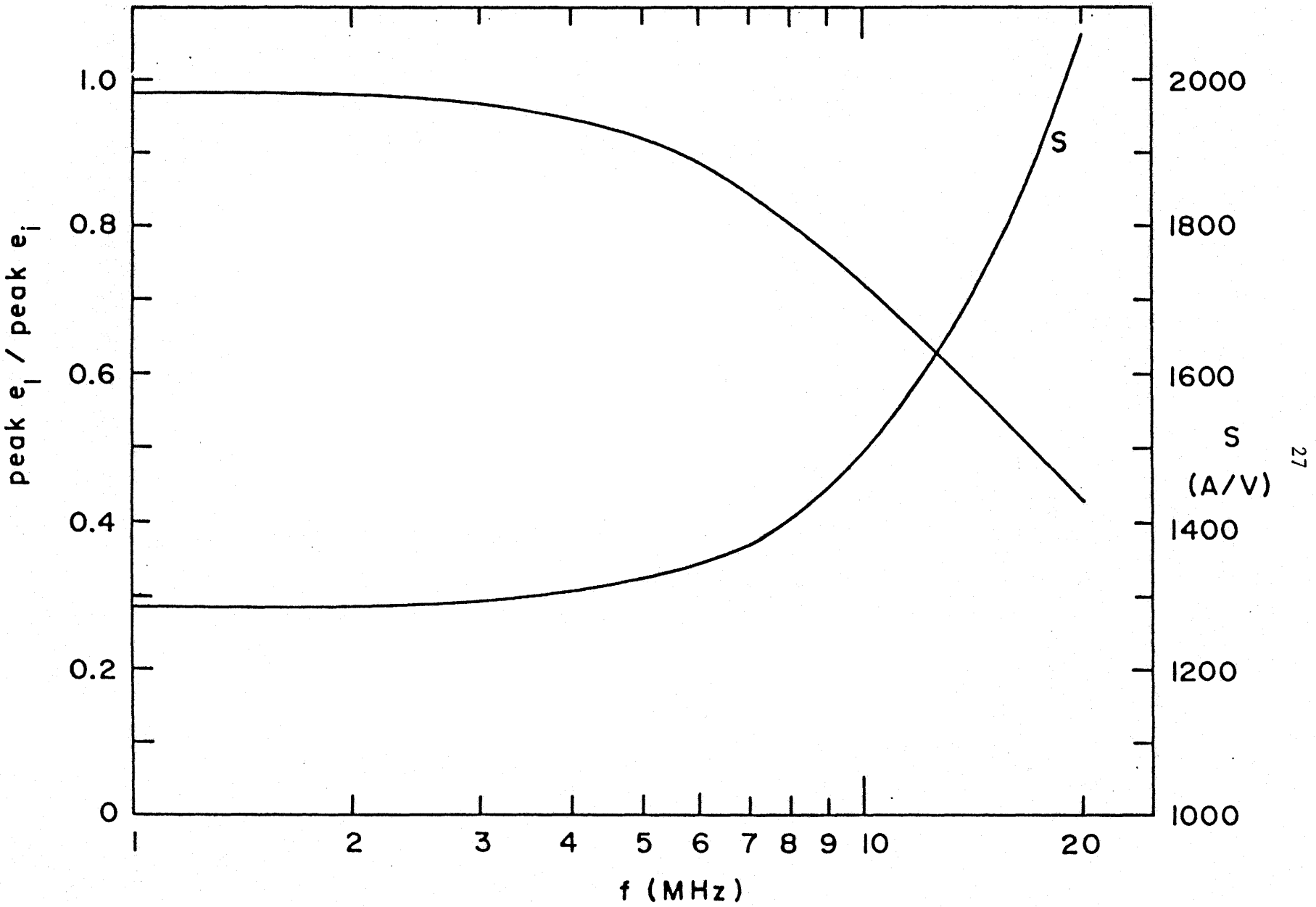

Fig. 3.6. Rogowski coil frequency response. e_1 is the amplitude of the output signal, e_i is the amplitude of the input signal and s is the sensitivity.

where di_p/dt is the time rate of change of the plasma current. This provides an approximate correction to the electric field for plasma inductance if there is no skin effect.

3.2.4 The microwave interferometer

The interferometer arrangement used is the same as described by Strilchuk (1971) except that the 10 db and 15 db horns connecting the crystal detector are reversed. The system is shown schematically in Fig. 3.7.

The phase shift $\Delta\phi$ of the 17 GHz microwave signal due to the presence of a plasma is given by

$$\Delta\phi = \cos^{-1}\left[\frac{1}{2}\sqrt{\frac{P_1}{P_2}}\left(\frac{P_3}{P_1} - \frac{P_2}{P_1} - 1\right)\right] \tag{3.2}$$

where P_1 is the power at the detector with the transmission arm cut off, P_2 is the power at the detector with the reference arm cut off and P_3 is the power at the detector with both the reference and transmitted signals present. Further, if the reference and transmitted powers are equal

$$\Delta\phi = \cos^{-1}\left[\frac{P_3}{2P} - 1\right] \tag{3.3}$$

where P is either the reference or transmitted power. The ratio P_3/P can be obtained from the output of the detector load resistor and the crystal calibration curve given in Fig. 3.8. The relationship is

$$\frac{P_3}{P} = 10^{0.1\,(R-R_3)} \tag{3.4}$$

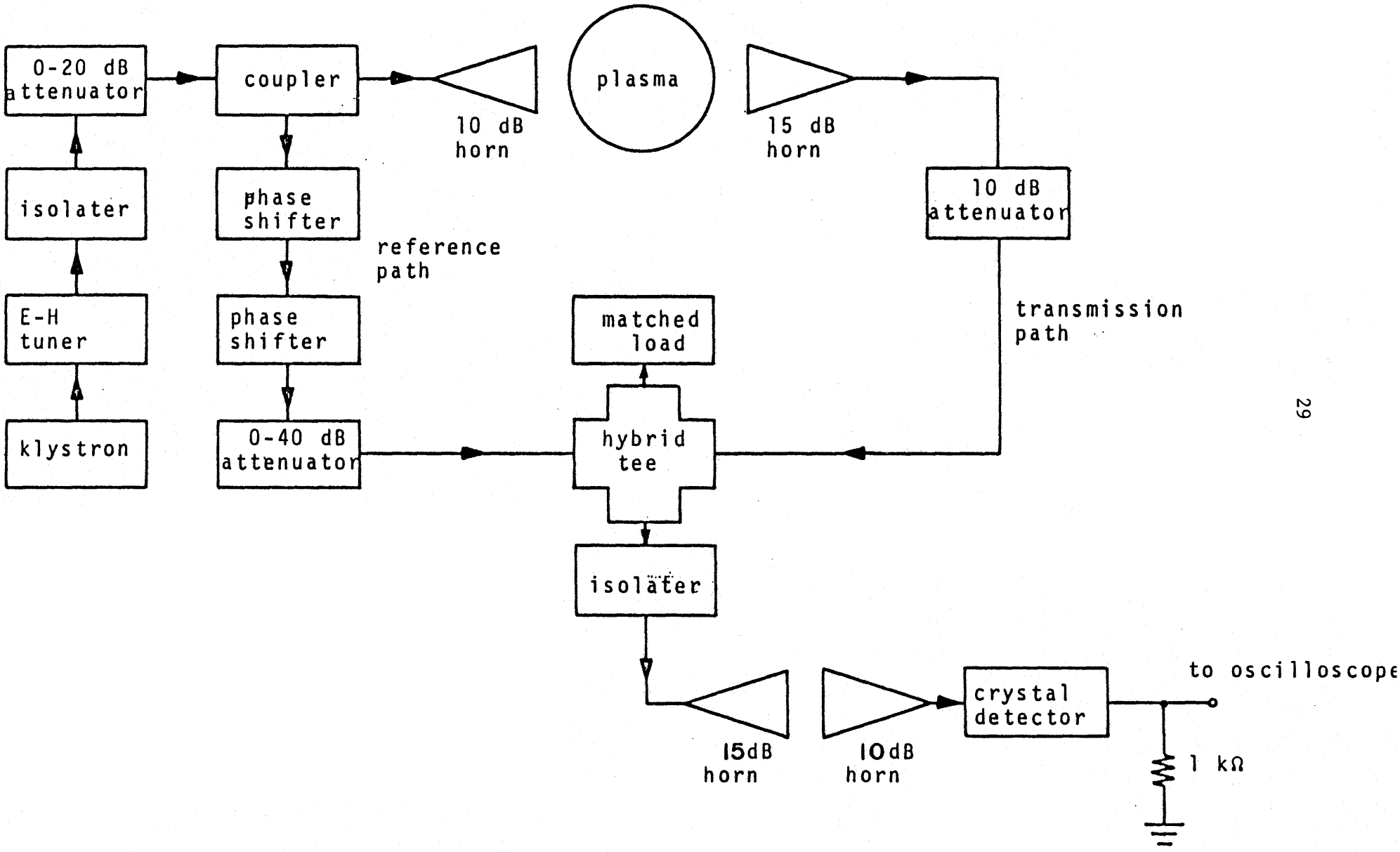

Fig. 3.7. Schematic diagram of the 17 GHz interferometer.

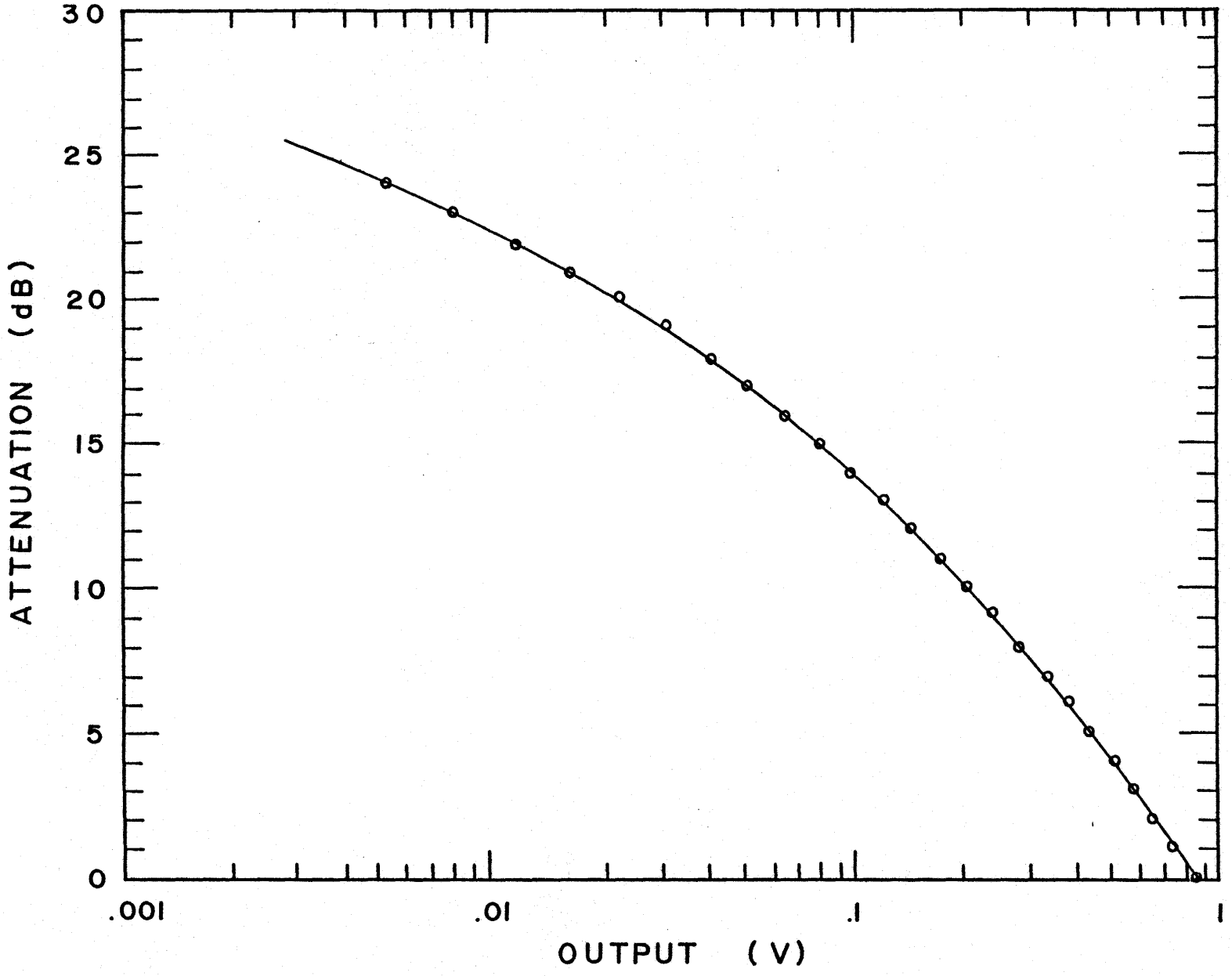

Fig. 3.8. Microwave crystal calibration curve (load resistance 1 kΩ).

where R is the value of the attenuation (in dB) corresponding to the voltage output when either arm is cut off, and R_3 is the value of the attenuation corresponding to the voltage output with both arms open.

The calibration curve is obtained using the precision attenuator located in the reference arm. The transmit arm is closed and the detector output is measured for different values of attenuation.

The average particle density n along the beam path is given by

$$n(m^{-3}) = 5.9 \times 10^{15} \Delta\phi \text{ (degrees)} \quad . \qquad (3.5)$$

This expression is valid for densities well below about 3.6×10^{18} m^{-3} (the cutoff density for our microwave frequency).

3.2.5 The charge-selective orbit analyzer probe

The charge-selective orbit analyzer probe (Loughran, Schott and Skarsgard 1967; Loughran 1968) used in this experiment is described in detail in Loughran (1968). A diagram of the collector end of the probe is given in Fig. 3.9. The probe was inserted into the plasma with the entrance slit parallel to the toroidal magnetic field B_ϕ. In this experiment the probe was oriented so as to receive only electrons. Due to the low thermal velocity of the ions, no measurement of the ion temperature could be made with this device.

The probe circuit used is shown in Fig. 3.10. The load resistance R_L was 1 KΩ. Since the probe in the presence of a plasma behaves as a current source the choice of load resistance is a compromise between a large signal to noise ratio and a fast output rise time. The measured capacitance of the probe and coaxial cable with

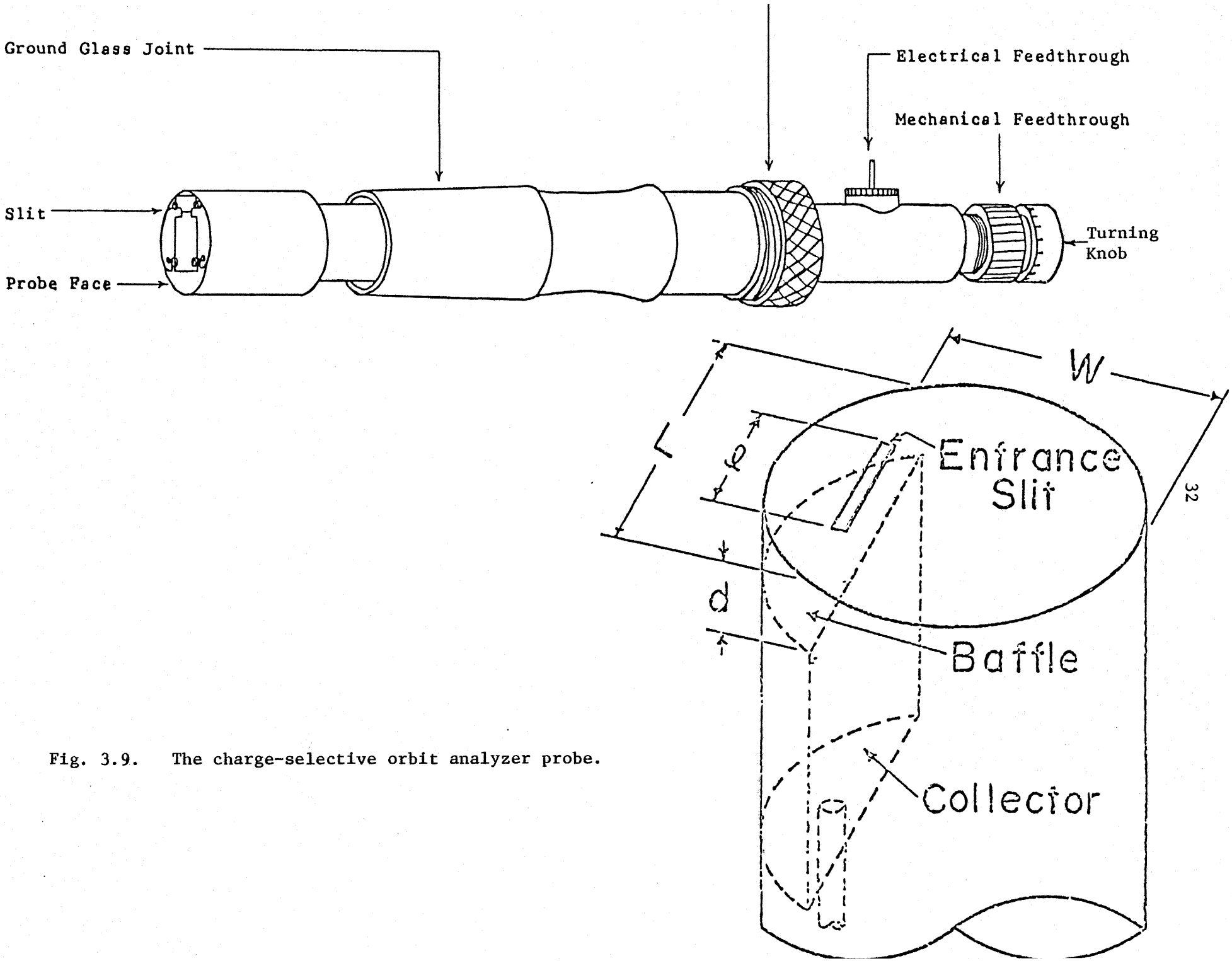

Fig. 3.9. The charge-selective orbit analyzer probe.

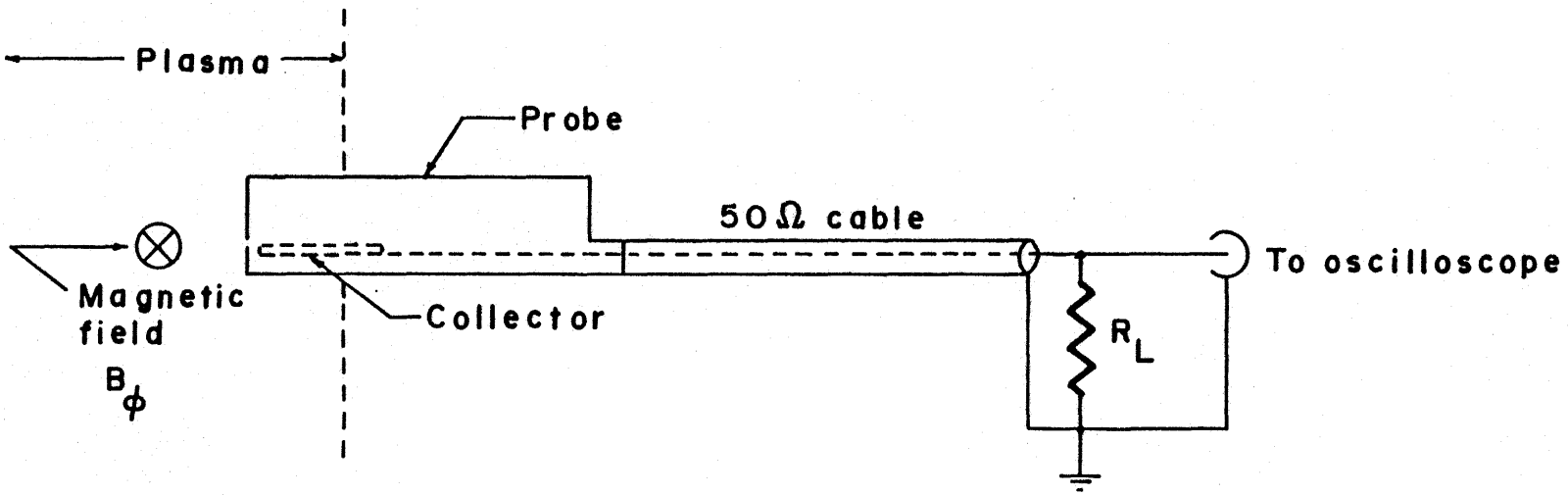

Fig. 3.10. Circuit diagram for the orbit analyzer probe (R_L = 1 kΩ).

no plasma present is 100 pF. This gives a rise time of about .1 μsec.

The slit to collector distance d could be varied by means of a screw adjustable from outside the plasma. This enabled us to determine electron temperatures in the following way. A plot of probe output voltage V as a function of d is made. The slope dV/d(d) of the resulting curve is then measured at a number of points. Then a graph of ℓn (dV/d(d)) versus d^2 is made. This will be a straight line if the electrons have a Maxwellian energy distribution. The slope m of this line is related to the electron temperature T_e as follows

$$a_o^2 = \frac{1}{4m} \tag{3.6}$$

$$\begin{aligned} T_e &= 1.02 \times 10^{15}\ a_o^2\ B_\phi^2 \quad (°K) \\ &= 8.80 \times 10^{10}\ a_o^2\ B_\phi^2 \quad (eV) \end{aligned} \tag{3.7}$$

where B_ϕ is given in tesla and a_o is in meters.

3.2.6 Electrostatic probes

Two types of electrostatic probes were used in this experiment. Both were constructed of semi-rigid coaxial cable heavily shielded with copper braid on the side exposed to the atmosphere. Two probes of the type shown in Fig. 3.11a were used in an attempt to verify wave propagation in the plasma. One probe was bent as shown and the other was straight. The second type of probe shown in Fig. 3.11b had a longer exposed tip and was used to boost the signal strength. It enabled us to follow the plasma oscillations after the end of the electric field

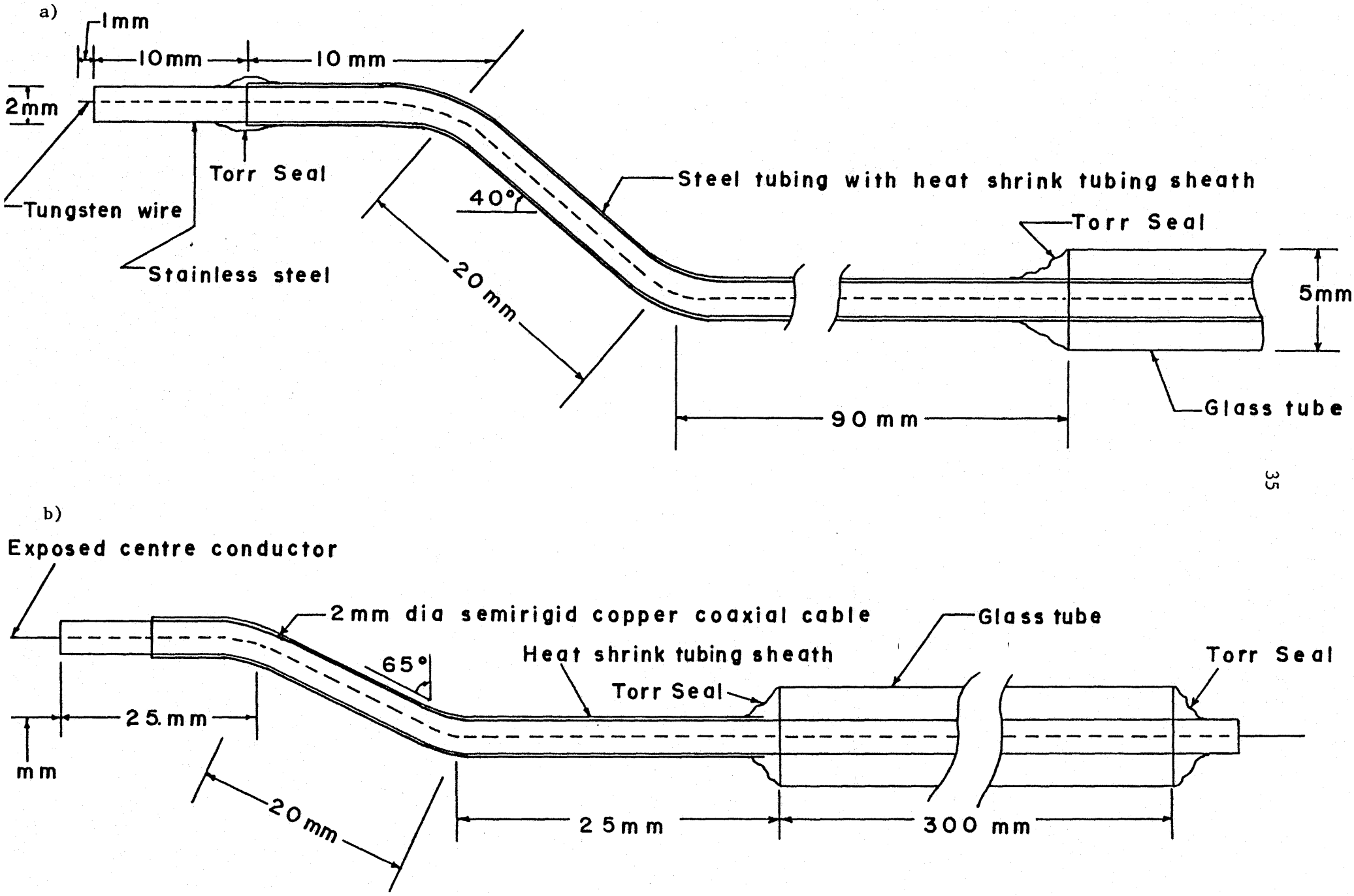

Fig. 3.11. Electrostatic probes. One of the probes used in an attempt to verify wave propagation is shown in a). The probe used to boost signal strength is shown in b).

pulse. Both types of probes were terminated with 50 ohms at the oscilloscope.

The approximate capacitance C of the second type of probe due to the presence of the plasma sheath was calculated from Crawford and Grard (1965)

$$C = 4\pi\varepsilon_o \left[\frac{m}{2M} \text{ EXP } \left(\frac{V_f}{-V_e}\right)\right]^{1/2} \left(\pi \frac{V_e}{V_f}\right)^{1/4} \frac{A_p}{4\pi\lambda_D} \tag{3.8}$$

where ε_o is the permittivity of vacuum, m is the mass of an electron, M is the mass of an ion, A_p is the probe area, λ_D is the plasma Debye length, V_f is the output voltage of the probe and

$$V_e = \frac{k\,T_e}{e} \tag{3.9}$$

where k is Boltzmann's constant, T_e is the electron temperature and e is the charge on the electron. For this experiment

$$\lambda_D = 1.7 \text{ mm}$$
$$V_f/V_e \simeq 1$$
$$A_p = 9.4 \text{ mm}^2$$

which yields a probe capacitance due to the plasma sheath of about 2×10^{-16} F. This is negligible when compared to the purely mechanical probe capacitance measured to be 1.2×10^{-10} F. The probe when terminated with 50 Ω has a corner frequency of about 1.7×10^8 rad/sec.

3.2.7 Floating double probe

Figure 3.12 is a diagram of the double probe used in the experiment to measure the electron temperature at the start of the electric field pulse. The measurement circuit was as shown in Fig. 3.13.

The electron temperature was determined from a plot of differential probe voltage as a function of probe current using the intercept method described in Johnson and Malter (1950). Briefly, the method is as follows.

The voltage developed across the 1 kΩ load resistor just before the electric field is applied is averaged for several discharges. This is repeated for many values of the probe potential difference V_d. The current characteristic is plotted and the following formula is used to find the electron temperature T_e.

$$T_e = 11{,}600\ (G - G^2)\left[\Sigma\, i_p \frac{dV_d}{di_d}\right]_{V_d=0} \qquad (°K) \qquad (3.10$$

or

$$T_e = (G - G^2)\left[\Sigma\, i_p \frac{dV_d}{di_d}\right]_{V_d=0} \qquad (eV) \qquad (3.11)$$

where Σi_p is the sum of the ion saturation currents, $[dV_v/di_d]_{V_d=0}$ is the resistance at $V_d = 0$ and

$$G = \frac{i_{e_2}}{\Sigma i_p} \qquad i_{e_2} = I - i_{p_2}$$

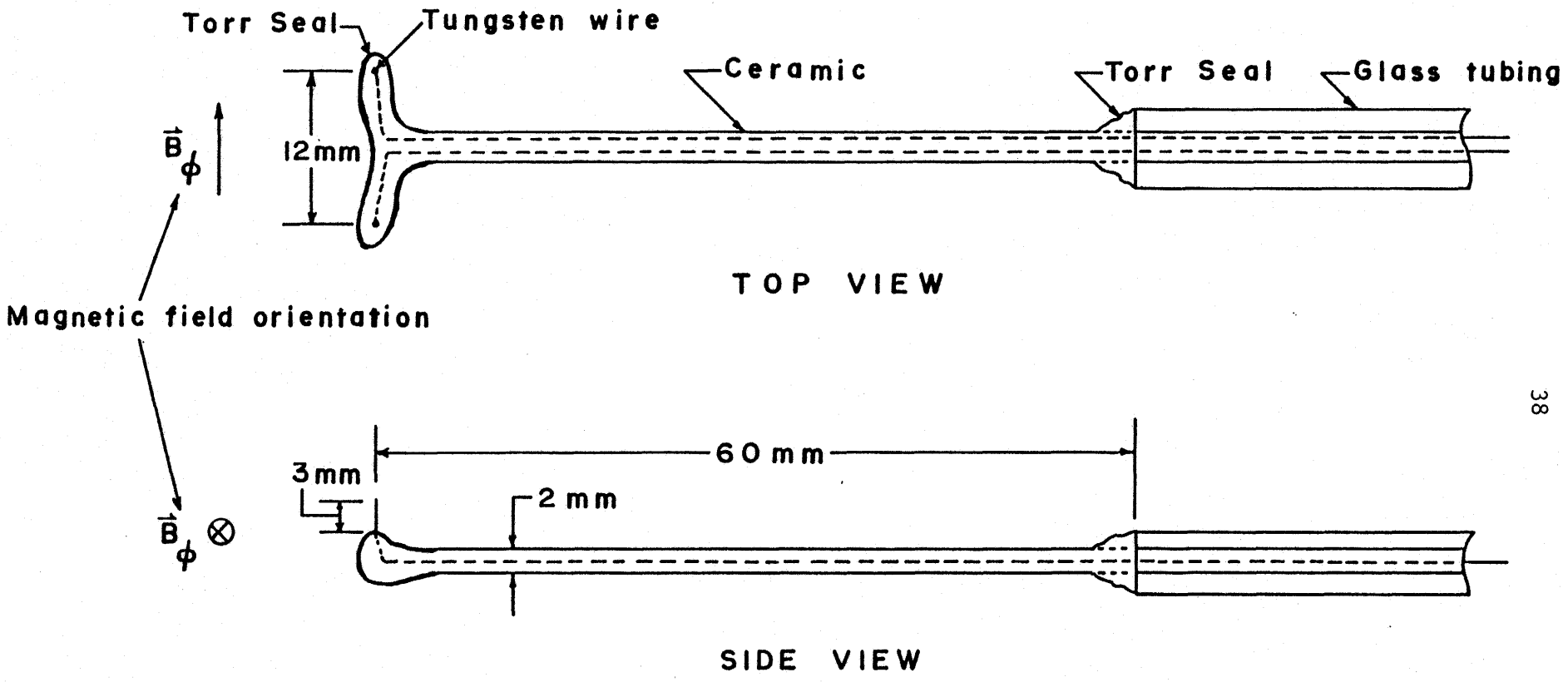

Fig. 3.12. The floating double probe. Toroidal magnetic field B_ϕ was oriented as shown.

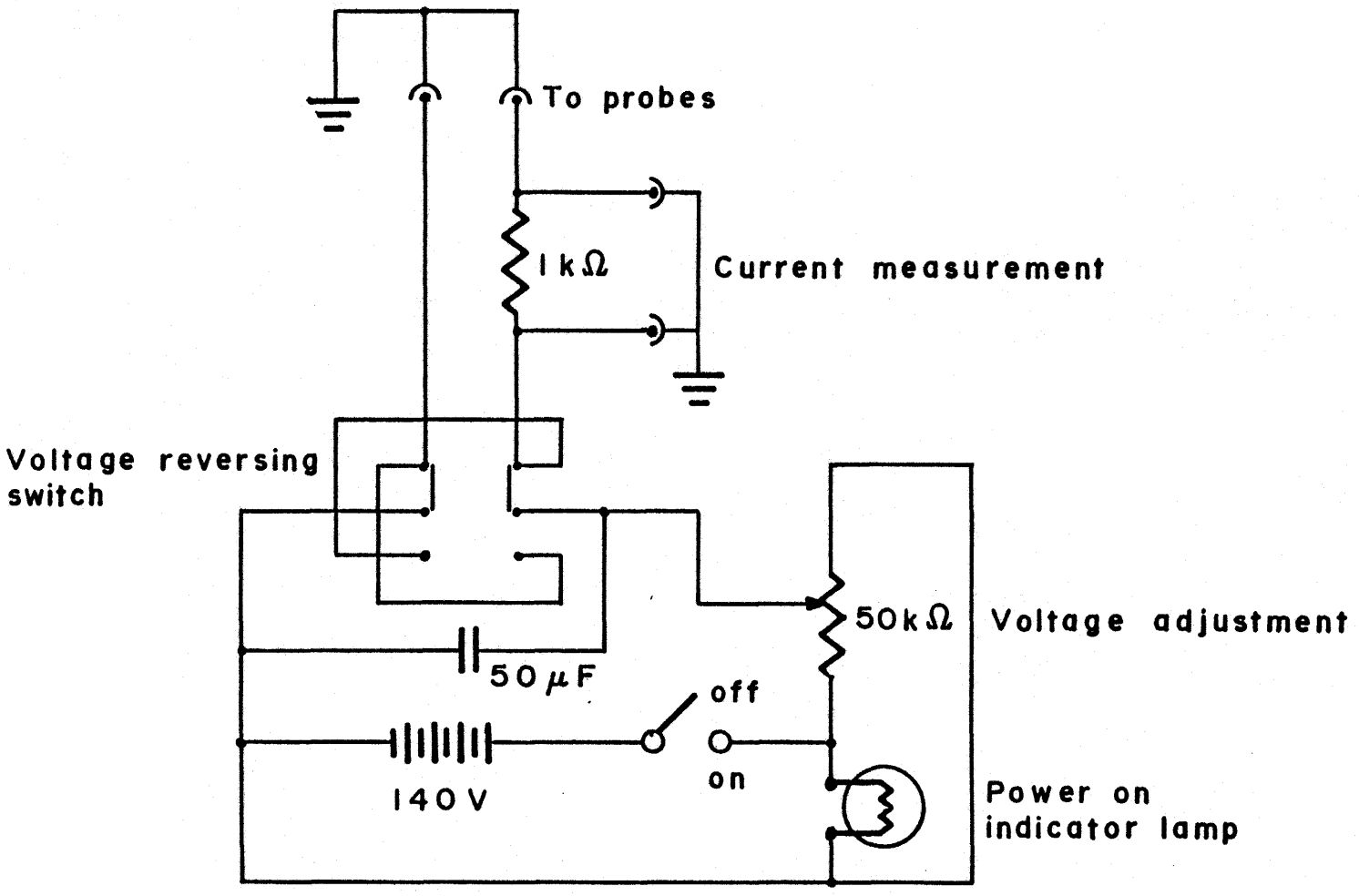

Fig. 3.13. Floating double probe circiutry.

where I is the probe current at $V_d = 0$ and i_{p_1} and i_{p_2} are as shown in Fig. 3.14.

It should be noted that the above method was developed for a collisionless, Maxwellian plasma in the absence of a magnetic field. The presence of the toroidal magnetic field could be expected to influence results but the effect is likely to be small if the probe is oriented as shown in Fig. 3.12.

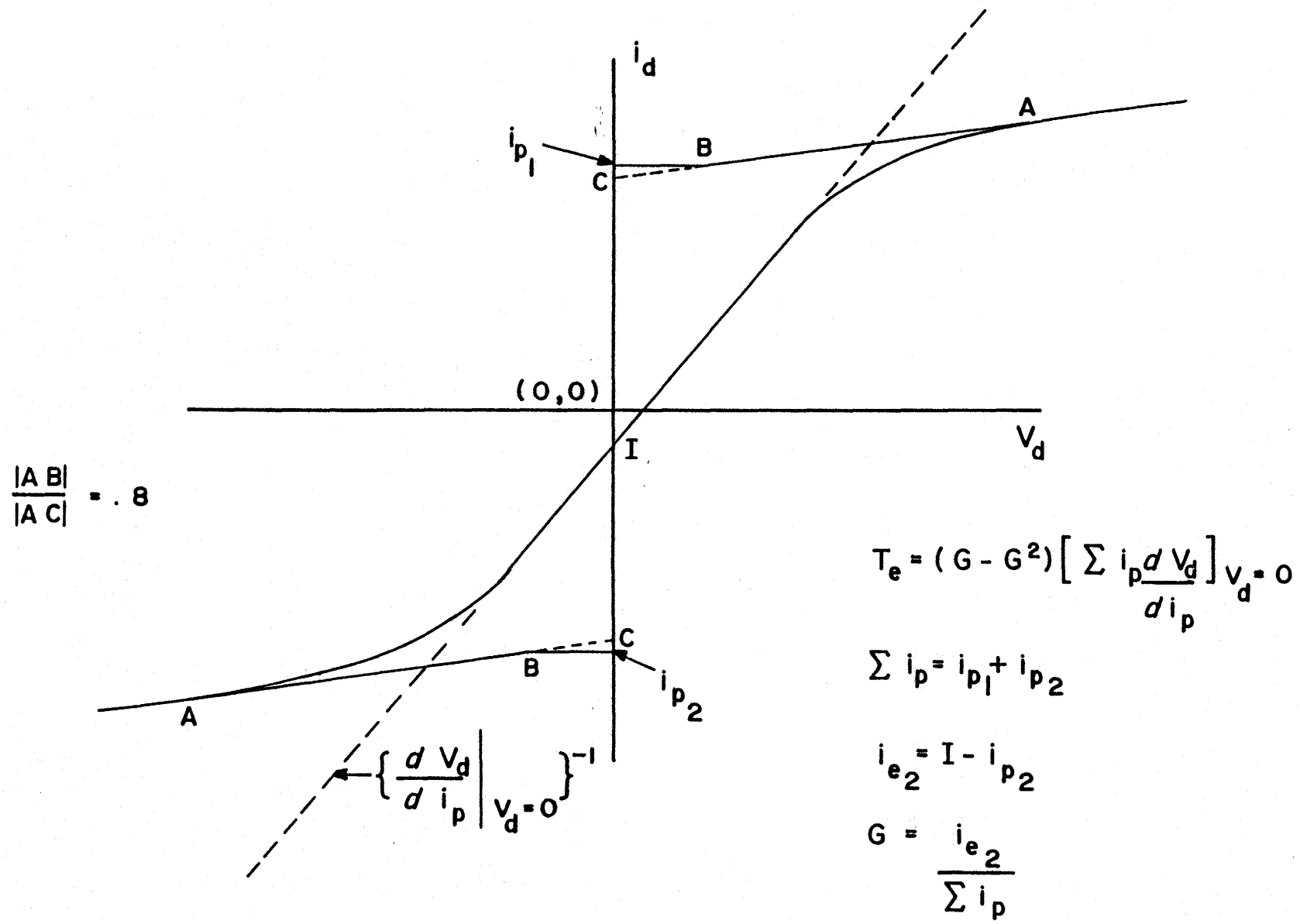

Fig. 3.14. Method used for analysis of the floating double probe current characteristic.

CHAPTER 4

EXPERIMENTAL RESULTS AND DISCUSSION

4.1 Introduction

A plasma which met the major criteria for the Buneman instability to occur was created. The measurements and calculations leading to the determination of the plasma parameters are given in this chapter. The electron drift and thermal velocities and overall energy conservation are given special attention. The variation in disruption time of the electron beam as a function of density is considered. A rough estimate of effective collision frequency as a function of time is given. The results of the electrostatic probe measurements are presented. Finally a comparison is made between experimental results and the theoretical work of Ishihara et al. (1980).

4.2 Achievement of the criteria for the Buneman instability

4.2.1 Introduction

The electron drift velocity determined from Rogowski coil data and density measurements shows that the drift velocity prior to the start of electron heating exceeded the minimum value needed for the Buneman instability to occur. The measured drift velocity will be compared to the velocity predicted by integrating the electric field as evidence in support of the existence of a period of free acceleration.

Results of the double probe measurement of initial electron temperature will be given in this section. The energy input into the

plasma will be determined and used to find the final electron temperature expected for no energy loss and complete thermalization of the electron drift energy. This final temperature will be compared to that measured with the orbit analyzer probe in an attempt to establish energy conservation.

It will also be shown that the radial boundary to the plasma should have little influence on the development of the instability.

4.2.2 Free acceleration and electron drift velocity

In order to achieve the objectives of this work it is important that the electrons be freely accelerated at early times. There can be no resistance if the drift velocity is to greatly exceed the thermal velocity of the electrons before the onset of turbulence. The observation of free acceleration will also show that there are no unexpected instabilities occurring on a shorter time scale than that predicted for the Buneman instability.

Figure 4.1 is a typical oscillograph of pickup loop voltage and Rogowski coil output. The effective electric field in the plasma may be found through Eq. 3.1. The electric field E_ϕ (corrected for dI_p/dt, shown in Fig. 4.2a) and the measured plasma current I_p for this discharge are shown as functions of time in Fig. 4.2b. The filling gas pressure was 5.6×10^{-4} Torr and the toroidal magnetic field at the centre of the torus was close to .2 T. A microwave density measurement performed on a similar discharge yielded a value of $(5.0 \pm .5) \times 10^{16}$ m^{-3} for the electron density n.

Two conclusions can be drawn if the electron drift velocity at

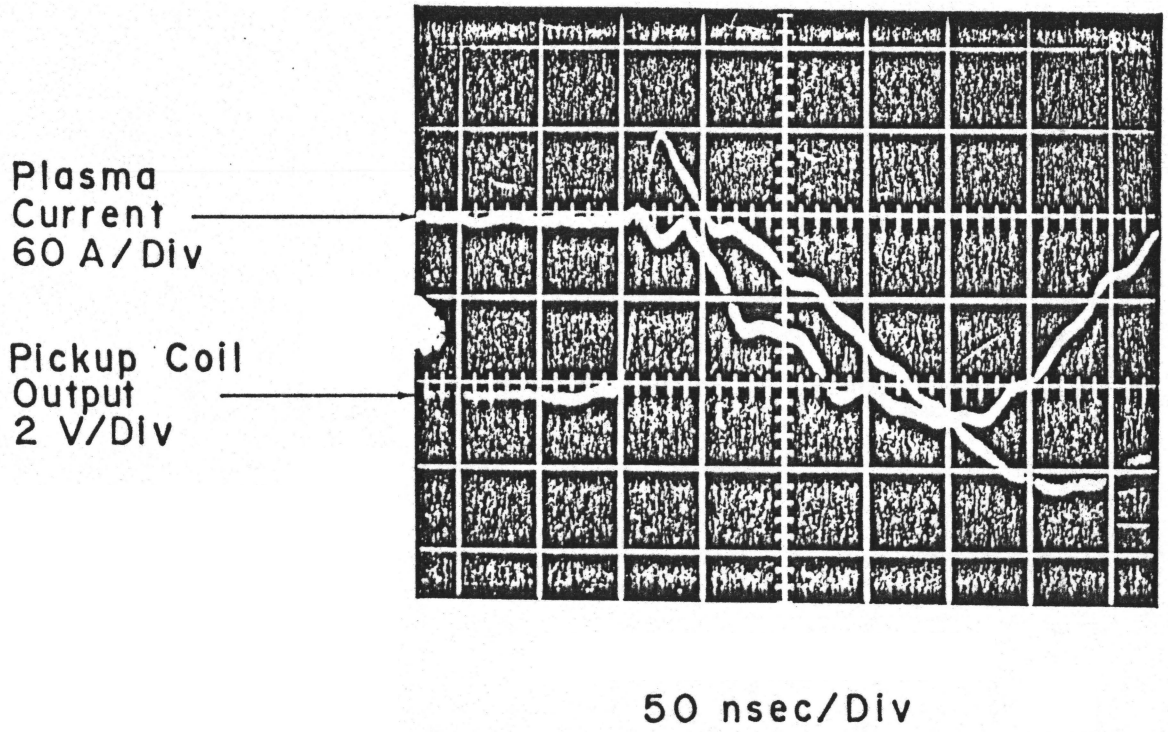

Fig. 4.1. Output of the pickup loop and Rogowski coil for a typical discharge with $n = 5.0X10^{16}$ m^{-3}.

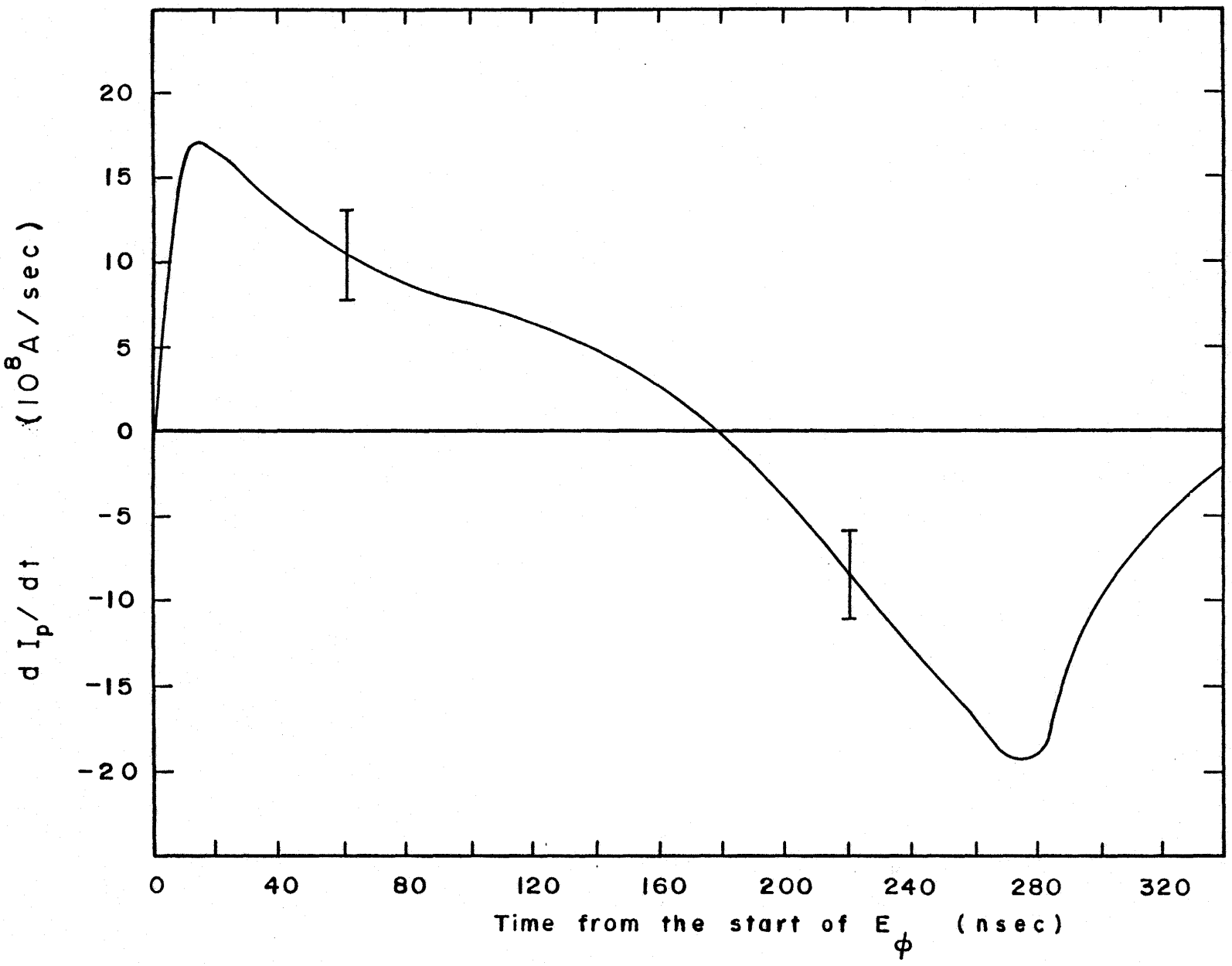

Fig. 4.2a. The rate of change of the plasma current for $n = 5.0 \times 10^{16}$ m^{-3} used in Eq. 3.1.

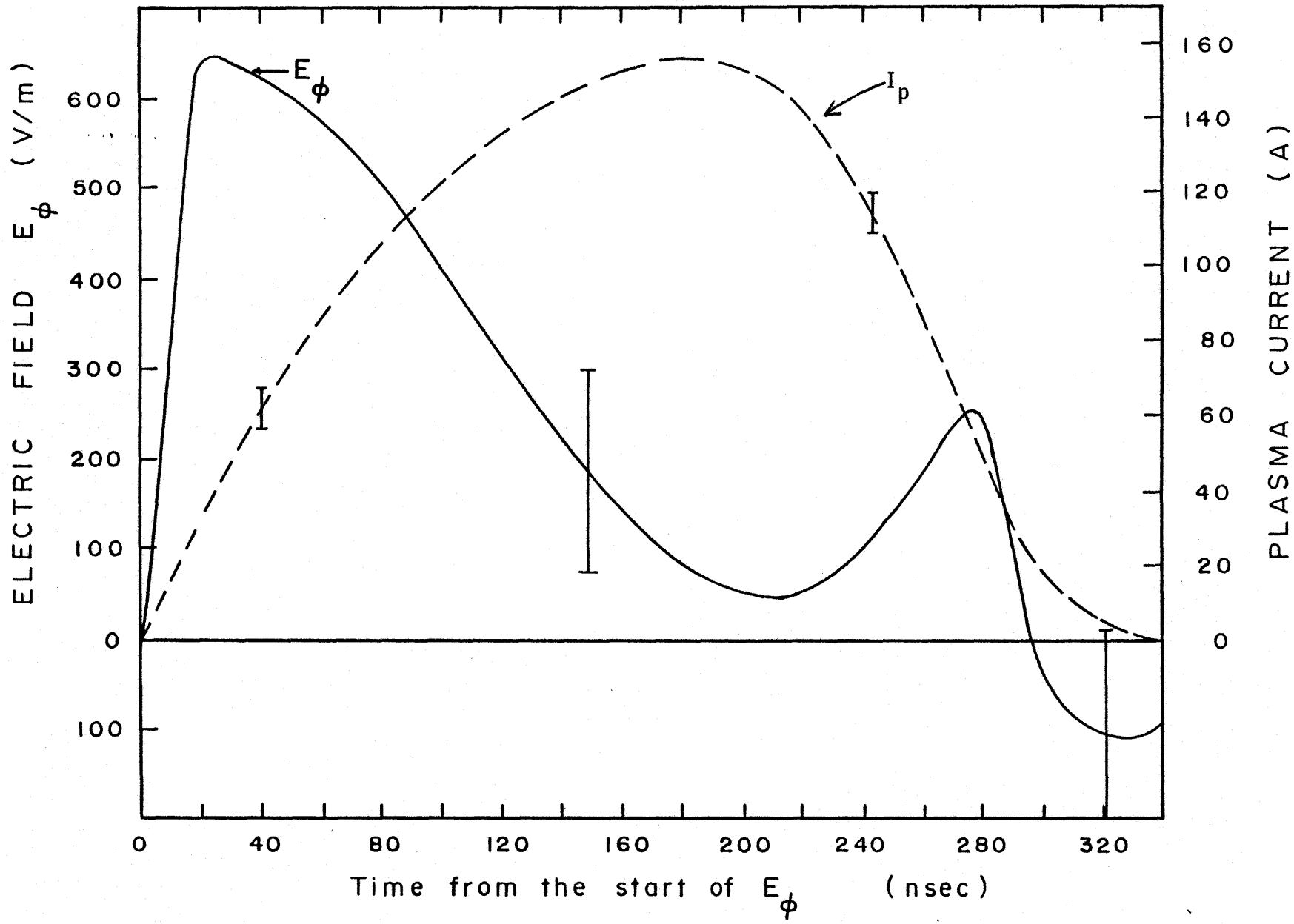

Fig. 4.2b. The applied electric field pulse and resulting plasma current for $n = 5.0 \times 10^{16}$ m^{-3}.

early times expected from only acceleration due to the electric field agrees with the drift velocity found from Rogowski coil data. There is a period of free acceleration and there is no stationary electron cloud. According to Strilchuk (1971) the plasma current is confined to a minor radius of 2.5 cm. The drift velocity of the electrons V_D is given by

$$V_D = \frac{I_p}{neA} \tag{4.1}$$

$$= \frac{I_p}{(5.0 \times 10^{16})(1.60 \times 10^{-19})(.025)^2\pi}$$

$$= (2.0 \pm .2) \times 10^5 \; I_p \; (\text{m/sec})$$

where e is the charge on an electron, A is the cross-sectional area of the current beam and I_p is the measured plasma current in Amperes.

If we assume free acceleration, the drift velocity of the electrons V_{FA} can be predicted from the electric field data.

$$[V_{FA}(t)] = \frac{e}{m} \int_{t_o}^{t} E_\phi(t')dt' \quad . \tag{4.2}$$

Here m is the mass of the electron, t_o is the time of the start of the electric field pulse and $E_\phi(t')$ is the strength of the electric field at time t'.

These two drift velocities are compared in Fig. 4.3. We see that there is reasonable agreement up until about 100 nsec after the start of the electric field pulse. This shows the absence of a stationary electron cloud.

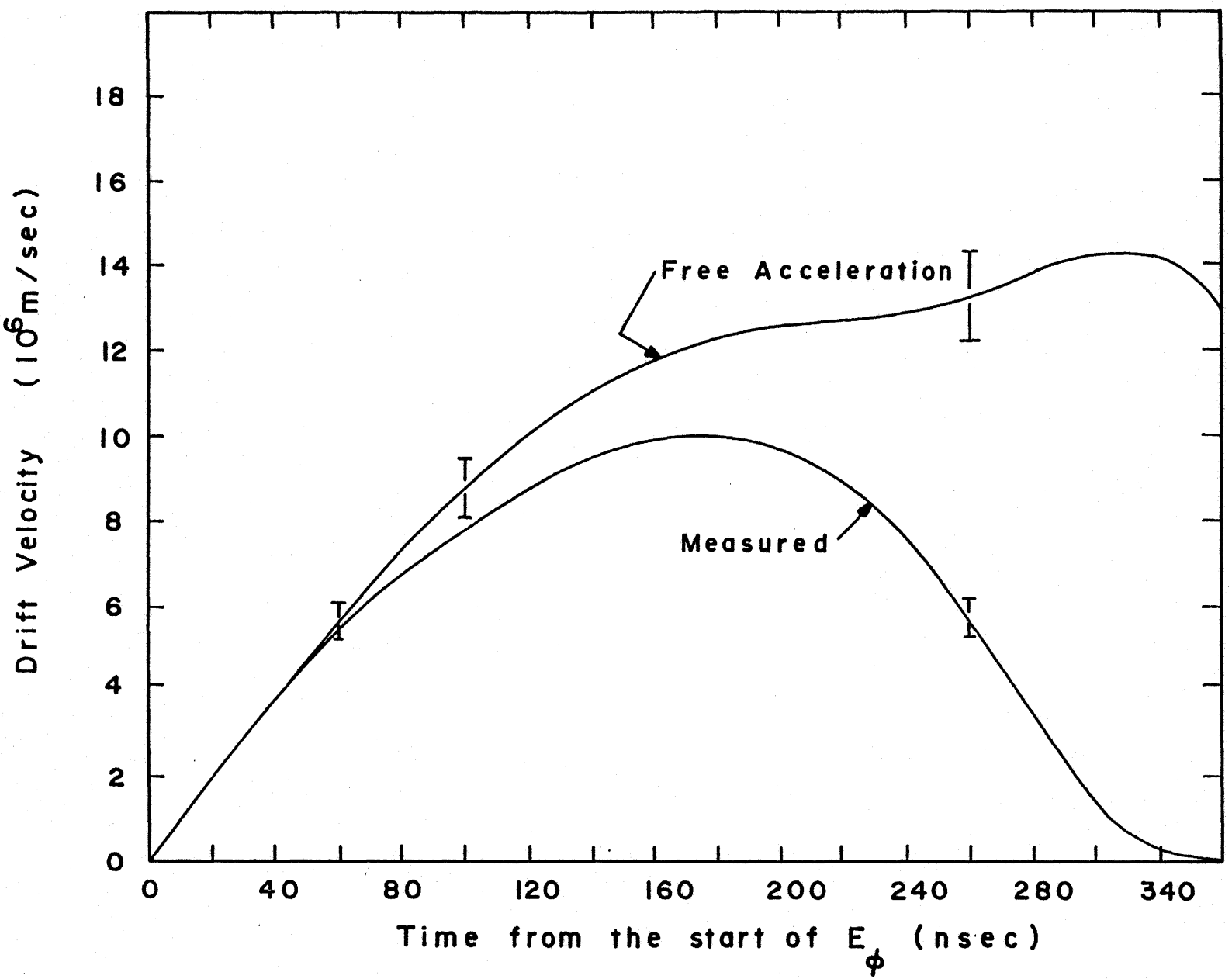

Fig. 4.3. Electron drift velocity as calculated from Rogowski coil data and expected free acceleration velocity as calculated from the E_ϕ curve for $n = 5.0 \times 10^{16}$ m^{-3}.

The output of the orbit analyzer probe also shows a delay of about 100 nsec between the application of the electric field pulse and the start of electron heating. Figure 4.4 shows a typical oscillogram of the probe's output. It should be noted that the rate of increase of temperature inferred from this figure is too slow due to the finite rise time (0.1 μsec) of the probe's output circuitry.

The above observations confirm that there was an interval of about 100 nsec of free acceleration by which time the drift velocity of the electrons had been boosted to around 7.8×10^6 m/sec. This is at least 5 times the initial thermal velocity of the electrons and the basic requirement of the Buneman instability is met. According to J.D. Jackson (1960) thermal effects should bring about a noticeable decrease in the growth rate predicted by Buneman for drift velocities less than approximately 5.5 times the initial thermal velocity. The nonlinear theory of Ishihara et al. (1980) was not intended to cover this less than ideal situation but the theory can still be expected to give a reasonably good description of the experiment.

4.2.3 Initial electron temperature measurement

The double probe characteristic obtained is shown in Fig. 4.5. The initial filling gas pressure was 5.6×10^{-4} Torr, the plasma electron density was about 5×10^{16} m^{-3} and the toroidal magnetic field had a magnitude of .2 T. Measurements were made immediately prior to the start of the applied electric field pulse. The rf preionization field had a duration of approximately 300 μsec. Each data point

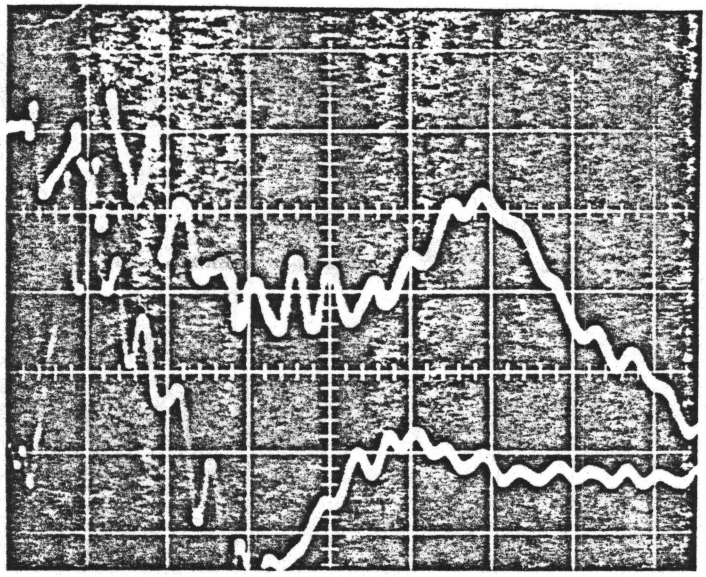

Fig. 4.4. Output of the orbit analyzer probe for a typical discharge.

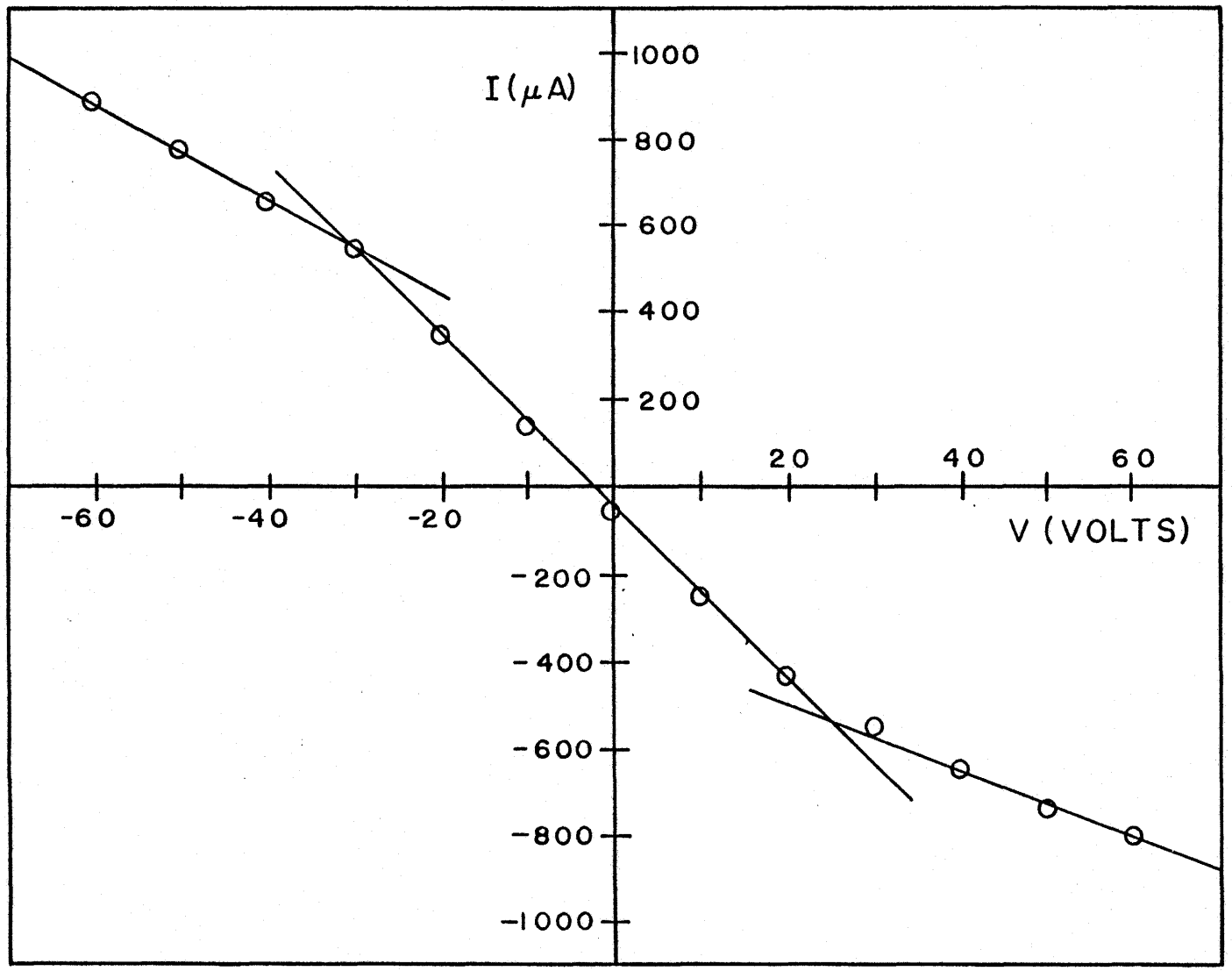

Fig. 4.5. Floating double probe current characteristic used to determine the initial temperature of the electrons.

is an average of four shots stored on a Tektronix 7834 storage oscilloscope. The curve is seen to be symmetrical and the method of electron temperature determination as given in Section 3.2.7 may be used.

The measured values for the quantities required in Eq. 3.10 are

$$i_{p_1} = 290 \pm 15 \ \mu A$$
$$i_{p_2} = -280 \pm 15 \ \mu A$$
$$I = -60 \pm 15 \ \mu A$$

$$\left.\frac{dV_d}{di_d}\right]_{V_d=0} = (5.0 \pm .6) \times 10^4 \ \Omega \ .$$

Therefore

$$i_{e_2} = 220 \pm 30 \ \mu A$$
$$\Sigma i_p = 570 \pm 30 \ \mu A$$
$$G = .39 \pm .07$$

The initial electron temperature is then 7 ± 2 eV, this corresponds to a mean initial thermal velocity of $(1.5 \pm .4) \times 10^6$ m/sec. This value is in rough agreement with those reported in Strilchuk (1971) for the Plasma Betatron.

4.2.4 Energy conservation

The charge selective orbit analyzer probe was used to measure the maximum temperature reached by the electrons. Electrical noise levels following the start of the electric field made it impossible

to use the double probe technique. Figure 4.4 shows a typical oscillograph of the output of the orbit analyzer probe. The output is characterized by a slow rise to an initial peak followed by a minimum and then a rise to a final larger peak. This final peak was present for every discharge but its shape, size and time of maximum value was not reproducible. The probe was located near the outer edge of the plasma where the electron density would change considerably if the plasma broke up. It is believed that this final maximum corresponds to the disruption of the plasma caused by the onset of instabilities. The initial peak is, however, quite reproducible and lends itself to the analysis given in Section 3.2.5. This indicates the presence of a Maxwellian velocity distribution, albeit only in the direction perpendicular to the magnetic field.

The probe output for several shots was stored on a Tektronix 7834 storage oscilloscope. The peak values were then averaged and the procedure repeated for other values of the slit to collector distance d. The data is illustrated in Fig. 4.6. Figure 4.7 is a graph of $\ell n[dV/d(d)]$ versus d^2 where V is the output of the probe in volts. The slope of the graph determined by linear regression is $-1.6 \pm .2\ mm^{-2}$; therefore

$$a_o^2 = - \frac{1}{4(-1.6\ mm^{-2})} = .16\ mm^2 \pm 10\% \quad .$$

The toroidal magnetic field B_ϕ, near the outer edge of the torus at the location of the orbit analyzer probe, was found to be related to the

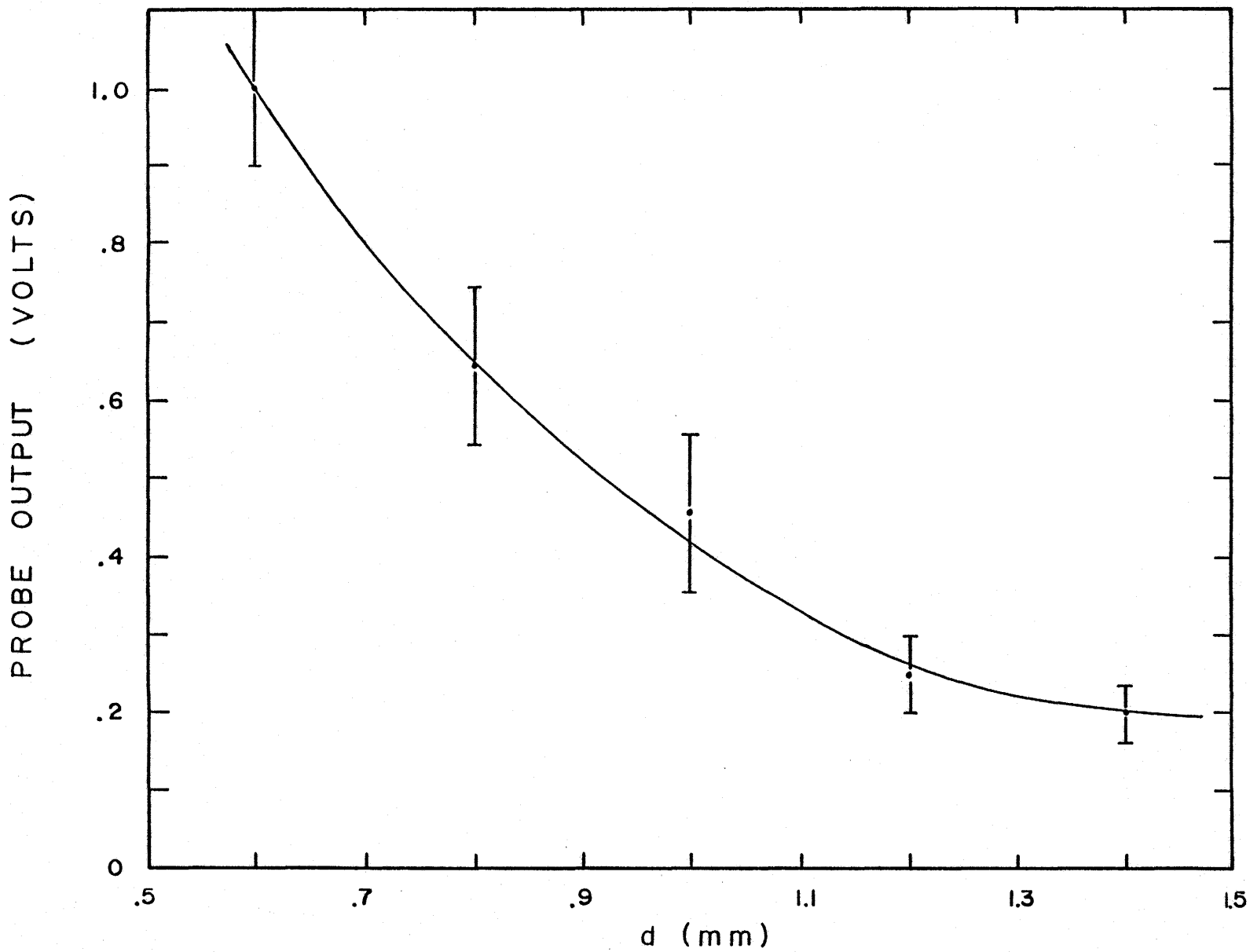

Fig. 4.6. Output of the orbit analyzer probe for different values of the slit to collector distance d.

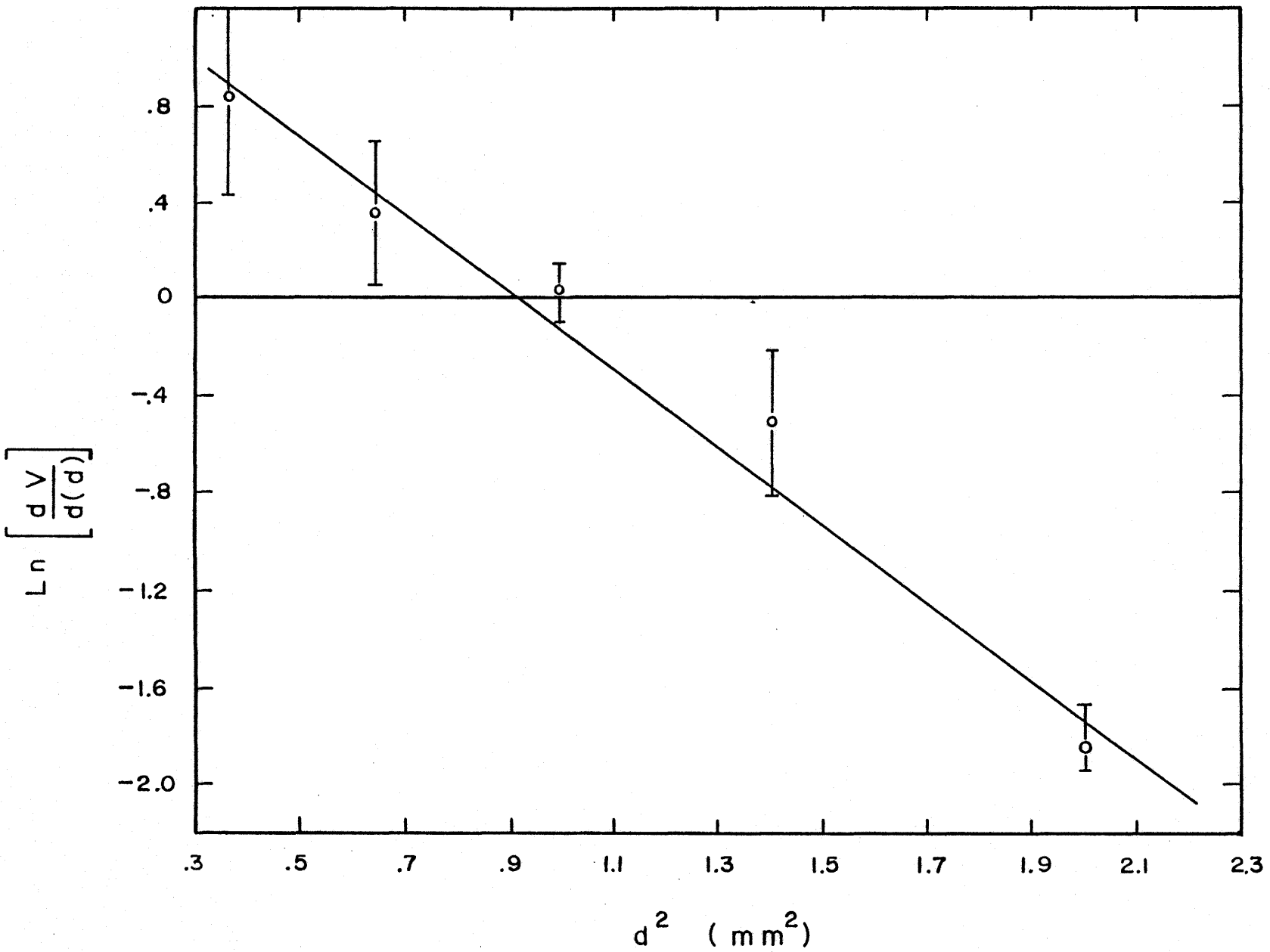

Fig. 4.7. Determination of Larmour radius a_o. Line shown is calculated by linear regression.

$$a_o^2 = \frac{-1}{4(\text{slope})}$$

current in the field coils by the ratio .645 ± .005 G/A. This value was determined by passing a DC current of 2.0 A through the coils and then measuring the resulting magnetic field with a Gaussmeter. There is a 2.0 mΩ resistor in series with the B_ϕ coils. It was used to measure the current in the coils (2.5 ± .1 × 10^3 kA) at the time of the application of the electric field pulse. The magnetic field therefore had a magnitude of 1.6 ± .1 kG or .16 ± .01 T. This datum together with Eq. 3.7 yields a final electron temperature of

$$T_{e_f} = 8.80 \times 10^{10} \ (.16 \times 10^{-6})(.16)^2$$
$$= 360 \pm 60 \text{ eV} \quad .$$

The time evolution of the thermal electron energy could not be followed because of the slow rise time of the output of the orbit analyzer probe and electrical noise. However, this process can be inferred if we assume energy was conserved. The energy balance equation is

$$\frac{3n(T_e(t)-T_{ei})}{2} + \frac{nmV_D^2(t)}{2} = en \int_0^t V_D(t) \ E_\phi(t) \ dt \qquad (4.3)$$

where e and m are the electron charge and mass, n is the electron density, T_e is electron temperature, T_{ei} is the initial electron temperature, V_D is the electron drift velocity, E_ϕ is the strength of the applied electric field and the integral over time is from the start of the electric field to time t.

Figure 4.8 illustrates the time variation of the electron thermal and drift energy densities. The electron density n was

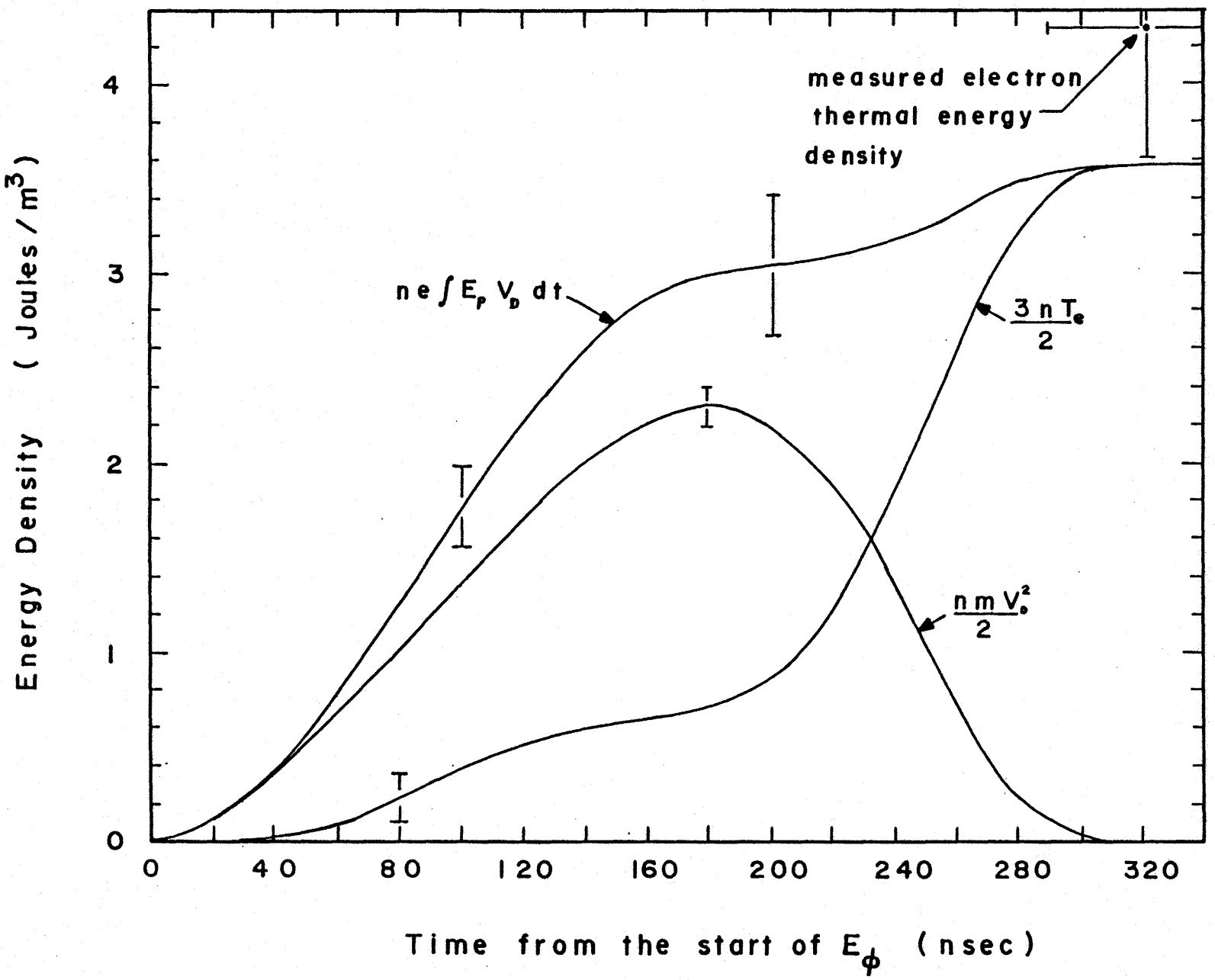

Fig. 4.8. Electron drift and thermal energy densities. Also plotted is the energy input into the plasma by the electric field pulse with $n = 5.0 \times 10^{16}$ m^{-3}. Measured electron thermal energy density shows good agreement.

5.0×10^{16} m^{-3}. The electron drift velocity data used is that shown in Fig. 4.3. The electric field data is given in Fig. 4.2. The electron thermal energy density was determined from Eq. 4.3. The final thermal energy density calculated from the orbit analyzer probe measurement

$$\text{Final thermal energy density} = \frac{3n\ T_{e_f}}{2} \text{ (measured)} \qquad (4.4)$$

is plotted in Fig. 4.8 for comparison. We note that Ishihara et al. (1980) predicts a small amount, ~10% of the input energy will go into field fluctuations; this is not taken into account in determining $T_e(t)$ from Eq. 4.3.

The agreement between the measured electron thermal energy density and that predicted by Eq. 4.3 indicates energy conservation until at least 340 nsec after the start of the electric field pulse. Moreover, it shows that all or most of the energy input was used in the isotropic heating of the electrons. This equal heating in all degrees of freedom was observed previously in the Plasma Betatron by Strilchuk (1971).

4.2.5 Boundary conditions and conclusions

The nonlinear theory discussed in Chapter 2 was developed for a boundary-free plasma. Since the plasma was toroidal in shape, there is no boundary along the magnetic field. The plasma was, however, radially bounded at a radius of about 2.5 cm. From the linear theory the wavenumber K of the dominant mode of the Buneman instability

is given approximately by

$$\frac{KV_D}{\omega_{pe}} = 1 \quad . \tag{4.5}$$

For an electron density of 5×10^{16} m^{-3} and an electron drift velocity of 7×10^6 m/sec, corresponding to the drift velocity at the end of the period of free acceleration, the wavelength λ of the dominant mode would be

$$\lambda = \frac{2\pi}{K} = \frac{2\pi}{2 \times 10^3 m^{-1}} = 3 \times 10^{-3} \text{ m} .$$

This is much less than the minor radius of the plasma column. Furthermore, as stated in Chapter 2, the growth rate is a maximum for modes propagating parallel to the toroidal magnetic field. The plasma dynamics are expected to be dominated by the fastest growing mode. The effect of the radial boundary is therefore likely to be small.

We have shown that the conditions necessary for the existence of the Buneman instability have been met. We have an interval of approximately 100 nsec of free acceleration which allows the electron drift velocity to exceed greatly the electron thermal velocity. This is followed by a fairly rapid and isotropic thermalization of the drift energy. We will show that this behaviour is consistent with that predicted for the Buneman instability by recent theory.

4.3 Electron beam disruption times

It is reasonable to assume that the length of time necessary for the instability to disrupt the plasma current would be dependent on some characteristic period of the plasma. The time between the peak in the plasma current and its destruction was measured for a number of different electron densities. The results are presented in Fig. 4.9. A density variation of from 4×10^{16} m^{-3} to 1.2×10^{17} m^{-3} was all that could be achieved by changing only the duration of the rf.

It is difficult to come to any conclusion, about the dependence of beam disruption time on density, from this graph. If anything, the disruption time seems to increase with increasing linear growth rate. This is contrary to what could be intuitively expected as the linear growth rate of the instability's dominant mode is proportional to $(\text{electron density})^{1/2}$. One should note that the electric field, as shown in Fig. 4.2 does not go to zero following the period of free acceleration but remains at a low value throughout the time of the plasma current. This could tend to delay the collapse of the current and reduce the dependence of decay time on density. One could also argue qualitatively that because of the plasma current inductance our device is current controlled at early times. That is, the current density $J = mnV_D$ tends to be a constant independent of plasma density. The drift velocity would therefore be smaller at higher densities and thermal effects would reduce the growth rate of the instability thus delaying the collapse of the current.

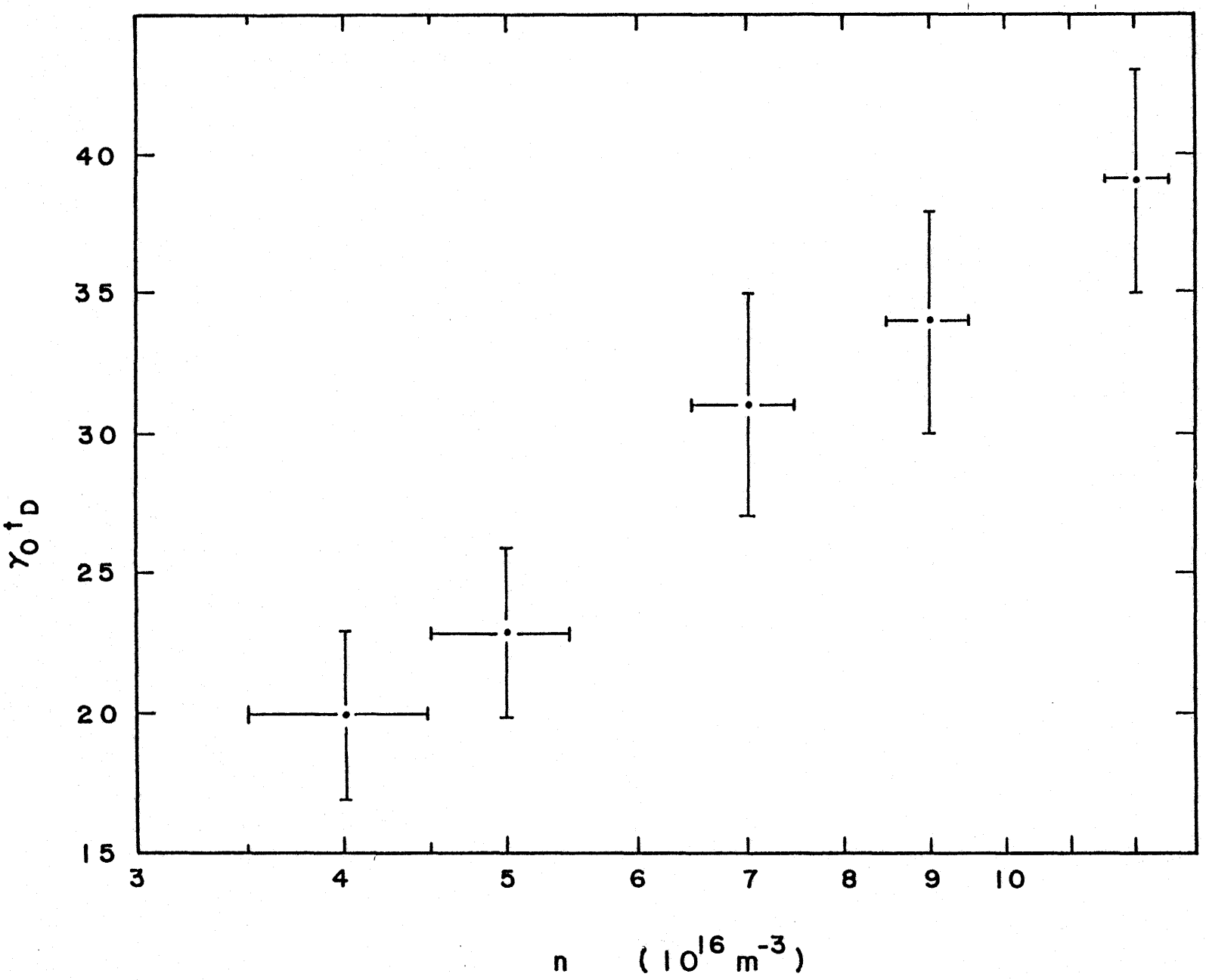

Fig. 4.9. Electron current beam disruption times. $\gamma_o t_D$ is the product of the maximum linear growth rate and measured current decay time. The nonlinear theory predicts $\gamma_o t_D = 7$.

4.4 Collision frequency

The classical electron-ion collision frequency ν for a plasma parameter can be calculated using (Spitzer 1956)

$$\nu_{classical} = \frac{ne^2\eta}{m} \tag{4.6}$$

where n is 5.0×10^{16} m^{-3}, e^2 is 2.6×10^{-38} C^2, m is 9.1×10^{-31} Kg and η is the classical resistivity equal to 6.5×10^3 $\ell n\ \lambda/T^{3/2}$ Ω-cm. For a temperature of 40 eV, or 4.6×10^5 °K, $\ell n\lambda$ is equal to 16. The classical collision frequency for electron-ion collisions is then

$$\nu_{classical} = 5 \times 10^3 \text{ sec}^{-1}$$

The actual effective electron-ion, electron-electron collision frequency ν_{eff} can be estimated from the force balance relation

$$m \left.\frac{dV_D}{dt}\right|_t = eE(t) - m\,\nu_{eff}(t)\,V_D(t) \quad . \tag{4.7}$$

Solving for ν_{eff} yields

$$\nu_{eff}(t) = \frac{eE(t) - m \left.\frac{dV_D}{dt}\right|_t}{mV_D(t)} \quad . \tag{4.8}$$

Here e and m are the charge and mass of the electron, V_D is the electron drift velocity, $dV_D/dt\big|_t$ is the acceleration of the electron at time t and E is the strength of the electric field. Figure 4.10 shows the time dependence of the collision frequency as deduced from the data presented in Fig. 4.2.

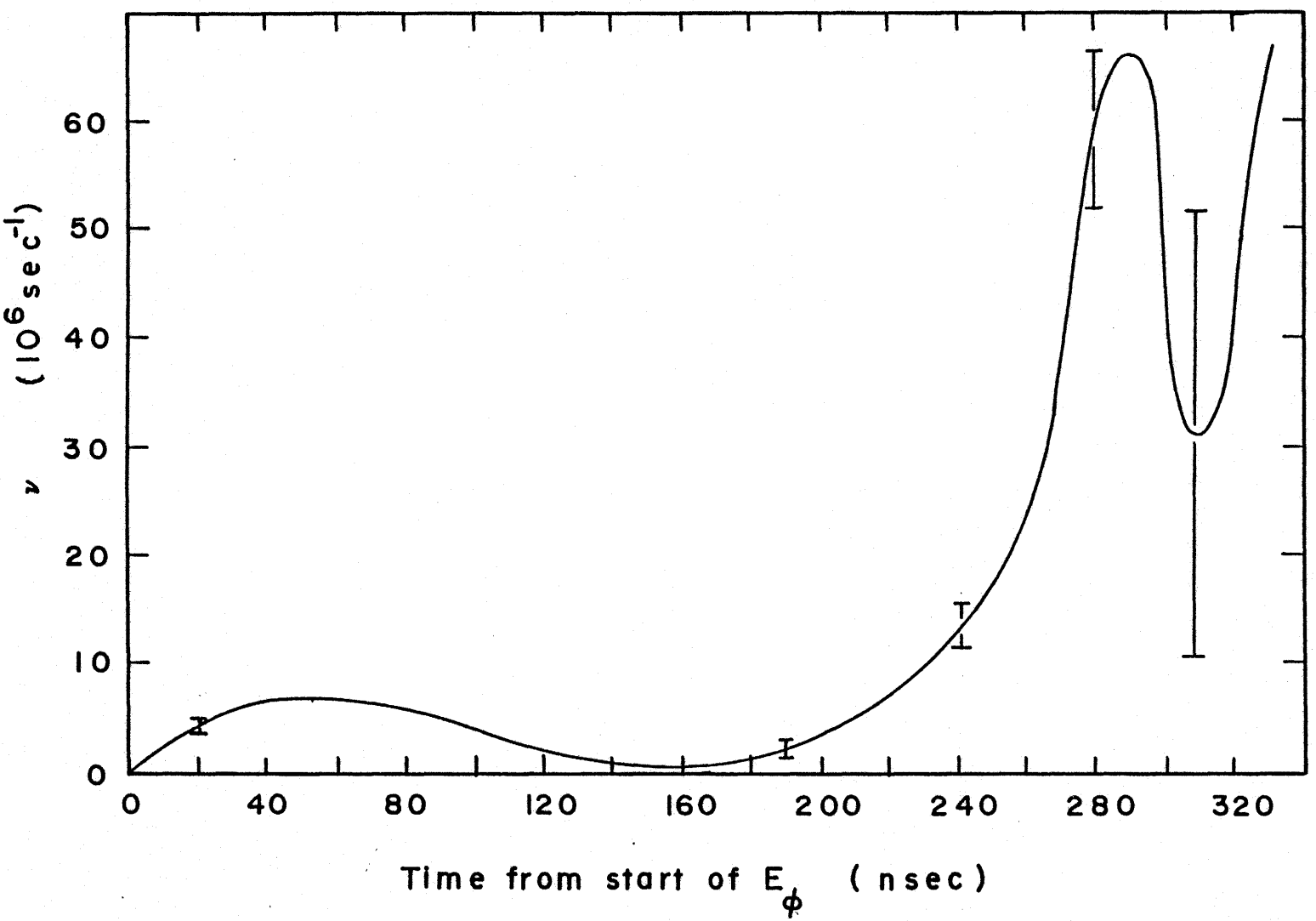

Fig. 4.10. Effective collision frequency as calculated from electric field and plasma current data for $n = 5.0 \times 10^{16}$ m^{-3}.

The collision frequency varies rapidly with time. The measured maximum collision frequency of about 6×10^7 sec^{-1} is a factor of 1×10^4 larger than the classical value.

The frequency of electron-neutral collisions was calculated using data from Brown (1959). This collision frequency ν_{e-n} is given by

$$\nu_{e-n} = p_o P_c V \tag{4.9}$$

where

$$p_o = \frac{273}{T} p \tag{4.10}$$

is the reduced pressure in Torr, T is the temperature in °K, p is the pressure of the filling gas in the torus, V is the velocity of the electrons and P_c is the collision probability for an electron-neutral collision. For a temperature of 293 °K, a gas pressure of 6×10^{-4} Torr, an electron velocity of 8×10^6 m/sec (the drift velocity at the departure from free acceleration), a value for P_c of 22 cm^{-1} $Torr^{-1}$ (Brown 1966), Eq. 4.9 yields

$$\nu_{e-n} = 1 \times 10^7 \text{ sec}^{-1} \quad .$$

This is only one-sixth of the measured maximum value. We would expect collisions with neutrals to have a noticeable effect while the drift velocity of the electrons is large and the level of the instability is still small. Figure 4.10 shows collision frequencies of this order of magnitude until the beginning of the fall of the plasma current

which occurs about 230 nsec after the application of the electric field pulse. Neutral collisions cannot explain the dramatic increase in collision frequency after this time.

4.5 Electrostatic oscillations

The single probes described in Section 3.2.6 were used to study electrostatic plasma oscillations for a range of electron densities from 4×10^{16} to 1.2×10^{17} m^{-3}. Figure 4.11 shows the output of one of the probes illustrated in Fig. 3.9a. At all densities investigated the probe output was characterized by low amplitude, high frequency oscillations to about t_o + 350 nsec, where t_o is the time of the application of the electric field pulse. This is followed by a rapid baseline shift and large amplitude, lower frequency oscillations.

The initial low amplitude oscillations are at the same frequency (~20 MHz) as the ringing in the spark gap trigger circuitry. When the Plasma Betatron was fired with too low a gas pressure to create a plasma these oscillations were still present but at a lower amplitude. This interference makes it impossible to extract information about plasma oscillations during the time of the electric field pulse.

After the pulse this interference becomes smaller and the signal becomes larger. The frequency of the oscillations after t_o + 350 nsec is plotted against electron density in Fig. 4.12. It should be noted that the uncertainty in measuring these frequencies is large as there were at most 1.5 to 2 oscillations after the decay of the current. Despite this, we see that the frequency increases

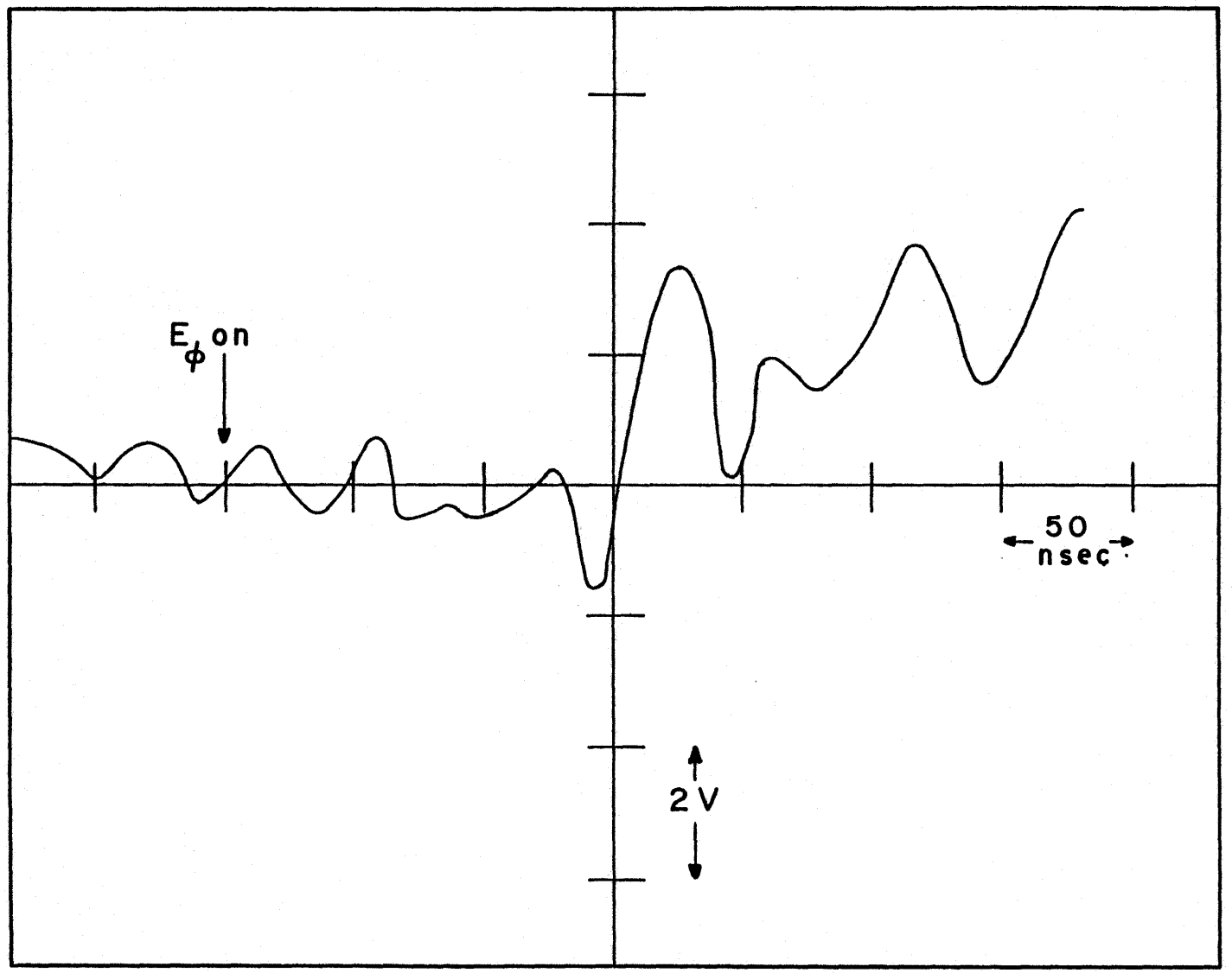

Fig. 4.11. Electrostatic probe output for an electron density of $n = 5.0 \times 10^{16}\ m^{-3}$.

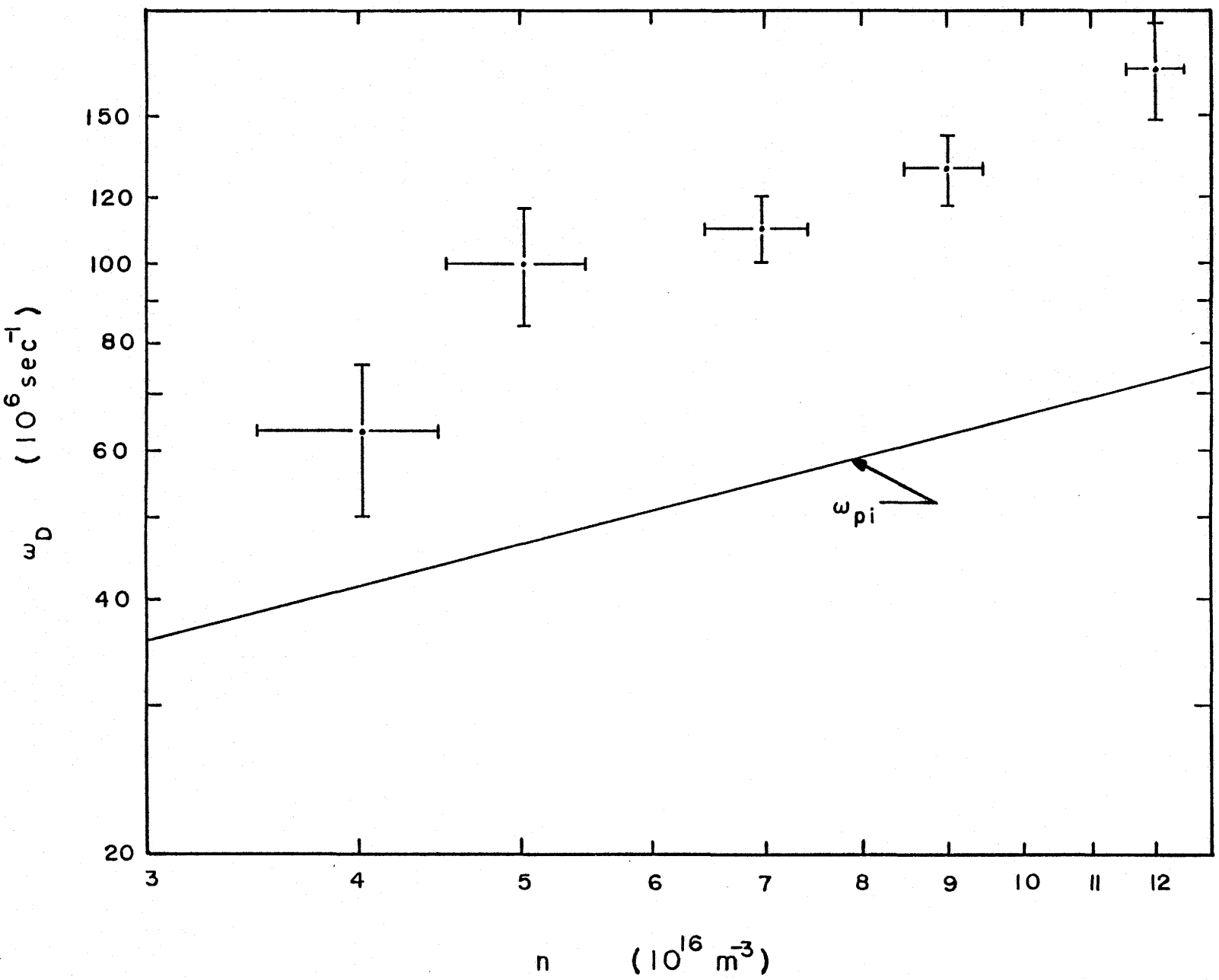

Fig. 4.12. Dominant frequency of observed oscillations after the collapse of the plasma current for several values of electron density.

significantly with density.

Using two of the bent probes and varying their separation an attempt was made to detect propagating electrostatic waves. We should have been able to detect wavelengths between 2 mm and 5 cm. No significant phase shifting between the probe outputs was observed either parallel to or across the toroidal magnetic field.

4.6 Discussion

The theory presented by Ishihara, Hirose and Langdon (1980) makes several predictions concerning the evolution of the Buneman instability. The drift energy of the electrons is, according to this theory, rapidly converted into thermal energy after 7 to 8 periods of the maximum linear growth rate γ_o. A low frequency ion sloshing motion, at the ion plasma frequency, and electron trapping are expected to begin at this time.

The current decay times shown in Fig. 4.9 yield an average value for $\gamma_o t_D$, where t_D is the time for current disruption, of about 30 . This is 4 times the predicted value of 7.5 $\gamma_o t_D$ (Section 2.2). The validity of this comparison is questionable for two reasons. First, we assumed the current decay time to be the time between maximum and zero plasma current. The theory assumes an initial drift velocity for the electrons while in reality they must be accelerated. The instability could begin at any time during this acceleration. Our choice of the plasma current maximum as a point of reference was somewhat arbitrary. Second, the theory was developed for an electric field

free plasma. In the experiment the electric field rises to 35% of its peak value at t_o + 290 nsec. The presence of this "residual" electric field could conceivably delay the collapse of the current beam by replacing some of the energy lost through the instability by the electrons.

Our graph of effective collision frequency indicates the possibility of electron-neutral collisions dominating near the end of the free acceleration period. The rapid current decay starting at about t_o + 250 nsec, indicated also by the sudden rise in collision frequency, may correspond to the onset of electron trapping predicted by theory. We can obtain an estimate of the collision frequency by applying Eq. 4.8 to the beam collapse predicted by computer simulation shown in Fig. 2.4.

$$\nu = \frac{eE - m \frac{dV_D}{dt}}{m V_D}$$

and if E = 0

$$\nu = \frac{1}{V_D} \frac{dV_D}{dt} = \frac{V_o^2}{2V_D^2} \frac{d}{dt}\left[\frac{V_D^2}{V_o^2}\right]$$

$$\simeq 2.0 \gamma_o \quad . \tag{4.7}$$

For an argon plasma with a density of 5×10^{16} m^{-3} the collision frequency would be $\sim 4 \times 10^8$ sec^{-1}. This is 6 times our peak measured collision frequency. The difference between theory and experiment can probably be attributed to thermal effects which would reduce the

growth rate and thus the violence of the instability.

The electrostatic oscillations observed after the decay of the plasma current have a dominant frequency of between 1.6 and 2.5 times the ion plasma frequency ω_{pi} as plotted in Fig. 4.12. They are, therefore, of the order of the ion plasma frequency and can likely be attributed to the predicted ion sloshing motion following the onset of electron trapping.

CHAPTER 5

SUMMARY AND CONCLUSIONS

This thesis has presented the results of an attempt to create experimentally the plasma conditions necessary for the development of the Buneman instability. A short, fast rising electric field pulse was applied to a cold toroidal plasma. This field was able to accelerate the electrons to a drift velocity several times their mean thermal velocity. The time variation of the plasma current and electric field was determined. The initial and maximum electron temperatures as well as the electron density were measured. Observations of electrostatic oscillations were carried out after the decay of the plasma current.

The following is a brief outline of the operation of the experimental system. A low pressure ($\sim 6 \times 10^{-4}$ Torr) argon gas flow is established in a toroidal glass vacuum chamber with a major radius of 19 cm and minor radius of 3 cm. A confining toroidal magnetic field ($\lesssim .2$ T) is produced by a capacitor discharge into coils spaced around the chamber. The fill gas is ionized by an rf (radio frequency) pulse. The length of this pulse is such that the desired plasma density exists when it is terminated at the time of maximum toroidal magnetic field. A short time (~60 μsec) after the end of the rf the electric field pulse is applied. The electric field is induced parallel to the magnetic field by specially placed coils mounted coaxial with the chamber. The plasma current rises to its maximum value approximately 180 nsec after the application of the electric field, then rapidly

decays to zero in approximately 120 nsec. The electrons are freely accelerated for approximately the first 100 nsec. Rapid electron heating is observed to begin at the end of the free acceleration period. The electron temperature reaches a maximum value close to 310 nsec after the start of the electric field pulse. This final thermal energy accounts for all of the energy input into the plasma by the electric field pulse.

The plasma current was monitored with a Rogowski coil and the electric field with a pickup loop. The electron density was measured with a 2 cm microwave interferometer. The electron temperature immediately before the electric field pulse was found using a floating double probe. The maximum electron temperature was determined with a charge selective orbit analyzer probe.

The existence and duration of the free acceleration period was determined in two ways. First, the actual electron drift velocity was found using electron density and current data. This velocity was compared to the expected electron velocity as calculated from electric field data assuming there was indeed free acceleration. There is good agreement between these two velocities until close to 100 nsec after the start of the electric field pulse. Second, the output of the orbit analyzer probe shows the start of electron heating was delayed approximately 100 nsec after the application of the electric field. This indicates there was no resistance to the plasma current flow for the first 100 nsec. A lack of resistance implies no collisions (or effective collisions) or free acceleration. At the end of this period of

free acceleration the electron drift velocity exceeded the electron thermal velocity by a factor (~5) which was sufficient to cause the onset of the Buneman instability.

The time variation of the electron thermal energy could not be followed directly. It could however be inferred from the energy input into the plasma by subtracting the electron drift energy. This naturally assumes that no energy was lost from the plasma. There was excellent agreement between the predicted final electron temperature and the maximum temperature measured with the orbit analyzer probe. The measured maximum temperature occurs at the end of the electric field pulse as expected. This agreement in both the magnitude and time of the maximum electron temperature indicates no loss of plasma energy until at least 340 nsec after the start of the electric field pulse.

Ours was essentially an unbounded plasma. Due to the toroidal geometry there was no boundary along the magnetic field. The minor radius of the chamber was much longer than the characteristic wavelength of the instability. For this reason the radial boundary should have had little influence on the instability's development.

Experimental results were considered in the light of a recent theoretical investigation (Ishihara, Hirose and Langdon 1980). This nonlinear theory is one-dimensional. The fact that the experimental system was three-dimensional is not expected to reduce the validity of the theory in our case. The linear growth rate was a maximum along the confining magnetic field and the plasma dynamics were expected to be dominated by the fastest growing mode. This fact tended to simplify

our system to only two dimensions.

Current decay times were measured for several plasma densities. The times were somewhat longer than those predicted by theory but were of the correct order of magnitude. The effective collision frequency exhibited a sudden rise near the end of the plasma current. Its peak value was four orders of magnitude larger than the classical (Spitzer 1956) value for our plasma conditions. This peaked behaviour is consistent with theory although the measured maximum value was several times less than the one predicted, probably because of thermal effects. The longer decay times can be attributed to differences between the experimental and theoretical systems. The theory assumes the electrons begin with an initial drift velocity sufficient to cause the Buneman instability. The instability is then allowed to develop in the absence of an electric field. In the experimental system the electrons must first be accelerated. The instability begins at some ill-defined time close to 100 nsec after the start of the electric field pulse. The electric field is still strong at this time. The field strength decays rapidly but rises to another peak (~35% of the first maximum) near the end of the plasma current as a result of imperfect crowbarring and current inductance. These differences make the current decay time comparison somewhat questionable.

It was noted that collisions between electrons and neutral particles could account for the measured collision frequency at early times. The sudden rise in collision frequency resulting in the collapse of the current beam cannot be explained in this way.

The theory predicts an ion sloshing motion at a frequency near twice the ion plasma frequency. Electrostatic oscillations with a frequency of a few times the ion plasma frequency were observed for several values of electron density. These oscillations began immediately following the collapse of the plasma current as predicted by theory.

We did not observe any dominant oscillation near the Buneman frequency ω_o defined in Eq. 2.3. A low amplitude wave existing before the collapse of the plasma current could have been masked by electrical noise. The absence of any dominant mode would however be consistent with the nonlinear theory. The theory predicts a very early and rapid shifting of the linear Buneman frequency due to nonlinear effects.

In conclusion, we created a plasma meeting all of the requirements for the Buneman instability to occur. There was complete thermalization of the electron drift energy over a time scale in agreement with theoretical predictions. The effective electron collision frequency behaves as predicted by theory. We failed to observe any dominant electrostatic mode near the Buneman frequency but we did observe a wave near the ion plasma frequency at later times.

REFERENCES

Bartlett, C.J. (1968) Phys. Fluids 11, 822.

Brown, S.C. (1959) Basic Data of Plasma Physics (The Massachusetts Institute of Technology and John Wiley and Sons Inc., New York) Chap. 1.

Budker, G.I. (1956) Dokl. Akad. Nauk SSSR 107, 807.

Buneman, O. (1959) Phys. Rev. 115, 503.

Crawford, F.W. (1965) J. Appl. Phys. 37, 180.

Dreicer, H. (1959) Phys. Rev. 115, 238.

Drummond, W.E., and Pines, D. (1962) Nucl. Fusion, Suppl. Pt. 3, 1049.

Gore, J.V. (1961) M.A. Thesis, University of Saskatchewan.

Hamberger, S.M., and Jancarik, J. (1972) Phys. Fluids 15, 825.

Hirose, A., and Alexeff, I. (1974) IEEE Transactions on Plasma Science Vol. PS-2, 222.

Hirose, A., and Ishihara, O. (1978) Plasma Physics Laboratory, University of Saskatchewan PPL-49.

Hirose, A., Mah, S.Q., Skarsgard, H.M., Strilchuk, A.R., and Whitfield, D.W.A. (1972) Phys. Rev. Letters 28, 1185.

Ichimaru, S. (1973) Basic Principles of Plasma Physics, A Statistical Approach (W.A. Benjamin Inc., Massachusetts) Chap. 9.

Iizuka, S., Saeki, K., Sata, N., and Hatta, Y. (1979) Phys. Rev. Letters 43, 1404.

Ishihara, O., Hirose, A., and Langdon, A.B. (1980) Plasma Physics Laboratory, University of Saskatchewan PPL-51.

Jackson, E.A. (1960) Phys. Fluids 3, 786.

Jackson, J.D. (1960) J. Nucl. Energy, Part C: Plasma Phys. 1, 171.

Johnson, E.O., and Malter, L. (1950) Phys. Rev. 80, 58.

Loughran, D.J. (1968) M.Sc. Thesis, University of Saskatchewan.

Loughran, D.J., Schott, L., and Skarsgard, H.M. (1967) Can. J. Phys. 45, 3055; also Plasma Physics Laboratory, University of Saskatchewan PPL-18.

Skarsgard, H.M., and Gore, J.V. (1965) Rev. Sci. Instrum. 36, 1807.

Skarsgard, H.M., and Reynolds, P. (1958) European Organization for Nuclear Research CERN 58-19.

Skarsgard, H.M., and Strilchuk, A.R. (1965) Bull. Am. Phys. Soc. 10, 214.

Spitzer, L. (1956) Physics of Fully Ionized Gases (Interscience Publishers Ltd., New York) Chap. 5.

Stefanovsky, A.M. (1965) Nucl. Fusion 5, 215.

Stix, T.H. (1962) The Theory of Plasma Waves (McGraw-Hill Book Company Inc., Toronto) Chap. 9.

Strilchuk, A.R. (1971) Ph.D. Thesis, University of Saskatchewan.

Tanaca, H., Hirose, A., and Koganei, M. (1967) Phys. Rev. 94, 161.

Vedenov, A.A., Velikhov, E.P., and Sagdeev, R.Z. (1962) Uspekhi fiz. Nauk (USSR) 73, 701.

Whitfield, D.W.A., and Skarsgard, H.M. (1974) Phys. Fluids 17, 2255.

APPENDIX A

DERIVATION OF THE LINEAR DISPERSION RELATION FOR THE BUNEMAN INSTABILITY IN THE PRESENCE OF A MAGNETIC FIELD

From kinetic theory the dispersion relation (Stix 1962) for electrostatic waves in a uniform plasma is

$$K^2 = \sum_s K_{D_s}^2 \left[1 + \xi_o \sum_{n=-\infty}^{\infty} e^{-\lambda} I_n(\lambda) Z_s(\xi_n)\right] \tag{A1}$$

where

$$K_{D_s}^2 = \frac{ne^2}{\varepsilon_o T_s} \tag{A2}$$

is the Debye wavenumber squared,

$$\xi_n = \frac{\omega - n\Omega_s}{K_{\parallel} \beta_s} , \tag{A3}$$

and

$$\lambda = \frac{K_{\perp}^2 T_s}{m_s \Omega_s} \tag{A4}$$

in which ω and K are the frequency and wavenumber of the wave, n_s is the number density of the plasma species s, e is the charge of the electron, T is the temperature, $K_{\parallel}$ and $K_{\perp}$ are the components of the wave vector either parallel or perpendicular to the uniform magnetic field $\vec{B}$, I_n is the modified Bessel function of integer order n, Z is the plasma dispersion function, m is mass, ε_o is the permittivity

of a vacuum, and

$$\Omega_s = \frac{eB}{m_s} \tag{A5}$$

is the cyclotron frequency of the species s, and

$$\beta_s = \sqrt{2T_s/m_s} \tag{A6}$$

is the thermal speed.

If we assume the plasma is cold we can make the approximations

$$Z(\xi) = -\frac{1}{\xi} - \frac{1}{2\xi^3} \tag{A7}$$

$$I_o(\lambda) = 1 \tag{A8}$$

$$I_{-1}(\lambda) = I_1(\lambda) = \frac{\lambda}{2} \tag{A9}$$

$$I_n(\lambda) = 0 \text{ for } n = -\infty \cdots -2,\ 2 \cdots \infty \tag{A10}$$

$$e^{-\lambda} = 1 - \lambda. \tag{A11}$$

Inserting the above into Eq. A1 yields

$$K^2 = -\sum_s K_{D_s}^2 \left[1 + \xi_o(1 - \lambda)\{Z(\xi_o) + \frac{\lambda}{2}\,(Z(\xi_1) + Z(\xi_{-1})\}\right] \tag{A12}$$

and neglecting terms like λ/ξ^2 this reduces to

$$K^2 = - \sum_s K_{D_s}^2 \left[- \frac{1}{2\xi_o^2} + \lambda - \frac{\lambda \xi_o}{2} \left(\frac{1}{\xi_1} + \frac{1}{\xi_{-1}} \right) \right] \quad . \qquad \text{(A13)}$$

If there is no magnetic field and the electrons are drifting with speed V_D in the rest frame of the ions

$$\xi_{o_i} = \xi_{1_i} = \frac{\omega}{K\beta_i} \qquad \text{(A14)}$$

$$\xi_{o_e} = \xi_{1_e} = \frac{\omega - KV_D}{K\beta_e} \qquad \text{(A15)}$$

and Eq. A13 becomes

$$K^2 = + \sum_s \left[\frac{K_{D_s}^2}{2\xi_o^2} \right] \qquad \text{(A16)}$$

or

$$2K^2 = \frac{2K^2 \omega_{pe}^2}{\omega - KV_D^2} + \frac{2K^2 \omega_{pi}^2}{\omega^2} \qquad \text{(A17)}$$

where

$$\omega_{p_s}^2 = \frac{ne^2}{\varepsilon_o m_s} \qquad \text{(A18)}$$

is the plasma frequency of species s. This reduces to the field free dispersion relation

$$1 = \frac{\omega_{pe}^2}{(\omega - KV_D)^2} + \frac{\omega_{pi}^2}{\omega^2} \quad . \qquad \text{(A19)}$$

However, if as in the Plasma Betatron there is a magnetic

field present the direction of propagation of the wave relative to the field must be considered.

If the wave is propagating at some angle θ to the magnetic field

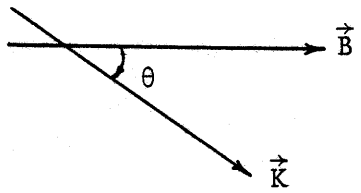

then

$$K_{\perp} = K \sin\theta \tag{A20}$$

$$K_{\parallel} = K \cos\theta \quad . \tag{A21}$$

If the electrons are drifting with speed V_D parallel to the magnetic field in the rest frame of the ions

$$\xi_{o_e} = \frac{\omega - K_{\parallel}V_D}{K\beta_e} \; ; \; \xi_{1_e} = \frac{\omega - K_{\parallel}V_D - \Omega_e}{K\beta_e} \tag{A22 & A23}$$

and

$$\xi_{o_i} = \frac{\omega}{K\beta_i} \; ; \; \xi_{1_i} = \frac{\omega - \Omega_i}{K\beta_i} \quad . \tag{A24 & A25}$$

Using these expressions in Eq. A13 gives

$$1 = \frac{\omega_{pe}^2}{(\omega - K_{\parallel}V_D)} \cos^2\theta + \frac{\omega_{pi}^2}{\omega^2} \cos^2\theta + \frac{\omega_{pe}^2 \sin^2\theta}{(\omega - K_{\parallel}V_D)^2 - \Omega_e^2} \tag{A26}$$

$$+ \frac{\omega_{pi}^2}{\omega^2 - \Omega_i^2} \sin^2\theta \quad . \tag{A26}$$

Equation A26 can be further simplified if

$$\Omega_e^2 >> \omega^2 >> \Omega_i^2 \quad . \tag{A27}$$

The equation then becomes

$$1 + \frac{\omega_{pe}^2}{\Omega_e^2} \sin^2\theta = \frac{\omega_{pe}^2}{(\omega - K_{\parallel} V_D)^2} \cos^2\theta + \frac{\omega_{pi}^2}{\omega^2} \quad . \tag{A28}$$

This is the linear dispersion relation for the Buneman instability in the presence of a uniform magnetic field.

Equation A27 can be rewritten as

$$\frac{\omega^4}{\omega_{pe}^4}\left[1 + \frac{\omega_{pe}^2}{\Omega_e^2}\sin^2\theta\right] - \frac{\omega^3}{\omega_{pe}^3}\frac{2K_{\parallel}V_D}{\omega_{pe}}\left[1 + \frac{\omega_{pe}^2}{\Omega_e^2}\sin^2\theta\right]$$

$$+ \frac{\omega^2}{\omega_{pe}^2}\left[\frac{K_{\parallel}^2 V_D^2}{\omega_{pe}^2}\left(1 + \frac{\omega_{pe}^2}{\Omega_e^2}\sin^2\theta\right) - \cos^2\theta - \frac{\omega_{pi}^2}{\omega_{pe}^2}\right]$$

$$+ \frac{\omega}{\omega_{pe}}\frac{2K_{\parallel}V_D}{\omega_{pe}}\frac{\omega_{pi}^2}{\omega_{pe}^2} - \frac{K_{\parallel}^2 V_D^2}{\omega_{pe}^2}\frac{\omega_{pi}^2}{\omega_{pe}^2} = 0 \quad . \tag{A29}$$

This fourth order in ω/ω_{pe} equation was solved for normalized growth rate γ/ω_{pe} as a function of $K_{\parallel} V_D/\omega_{pe}$. The densities of the electrons and ions were assumed equal so

$$\frac{\omega_{pi}^2}{\omega_{pe}^2} = \frac{1}{40(1836)} \tag{A30}$$

for an argon plasma. In our experiment the ratio ω_{pe}^2/Ω_e^2 was between .10 and .31. A value of .13 corresponding to a density of 5.0×10^{16} m^{-3} and a magnetic field strength of .2 T was used in the solution. Figure A1 shows that the growth rate is a maximum for $\theta = 0°$.

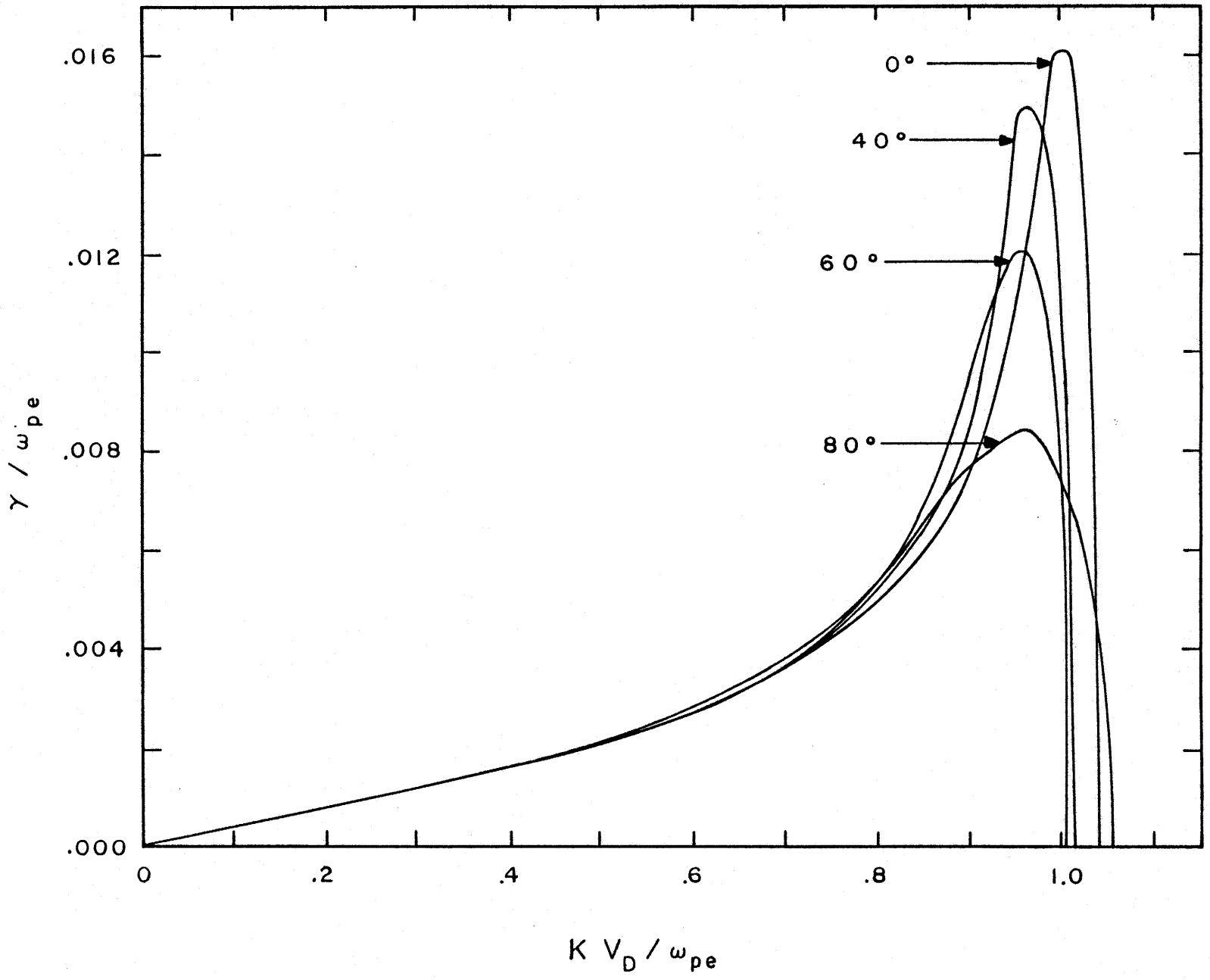

Fig. A1. Normalized linear growth rate as a function of normalized wavelength for several values of $\vec{K} \cdot \vec{V}/KV$.

APPENDIX B

PREDICTION OF THE BUNEMAN INSTABILITY'S DOMINANT MODE HALF-WIDTH

The time evolution of the instability's electric field energy $W_E(K)$ is given by

$$W_E(K) = E_i^2 \, e^{2\gamma(K)t} \tag{B1}$$

where E_i is the initial fluctuation level and t is time. If we consider the half-width of the peak in Eq. B1 a relationship between the maximum growth rate γ_o, the growth rate at one-half the maximum field energy $\gamma_{1/2}$ and time can be obtained.

$$\frac{E_i^2}{2} e^{2\gamma_o t} = E_i^2 \, e^{2\gamma_{1/2} t}$$

$$e^{2(\gamma_o - \gamma_{1/2})t} = 2$$

$$\gamma_o - \gamma_{1/2} = \frac{\ell n 2}{2t} \quad . \tag{B2}$$

If we expand γ near γ_o using Taylor's series we have

$$\gamma(K) \simeq \gamma_o + \frac{(\delta K)^2}{2} \frac{\partial^2 \gamma}{\partial K^2} \tag{B3}$$

since $\partial\gamma/\partial K = 0$ at $\gamma = \gamma_o$. Here δK refers to a small change in wave-number. Substituting this expression for $\gamma(K)$ into Eq. B2 for $\gamma_{1/2}$ yields

$$\gamma_o - \gamma_o - \frac{(\delta K)^2}{2} \frac{\partial^2 \gamma}{\partial K^2} = \frac{\ell n 2}{2t}$$

$$(\delta K)^2 = \frac{-\ell n 2}{[\partial^2 \gamma / \partial K^2] t}$$

$$\delta K = \sqrt{\frac{\ell n 2}{-[\partial^2 \gamma / \partial K^2] t}} \quad . \tag{B4}$$

δK now refers to the half-width of the electric field energy peak.

Hirose (1978) gives $\partial^2 \gamma / \partial V_D^2 = -4\ \omega_{pe} / V_D^2$ near $\gamma = \gamma_o$ where V_D is the drift velocity of the electrons and ω_{pe} is the electron plasma frequency. We need to convert this to a derivative with respect to K.

$$\frac{\partial^2}{\partial V_D^2} \equiv \frac{\partial}{\partial V_D} \frac{\partial}{\partial V_D} \equiv \left(\frac{\partial K}{\partial V} \frac{\partial}{\partial K} \right)^2 \equiv \left(\frac{\partial K}{\partial V} \right)^2 \frac{\partial^2}{\partial K^2}$$

and at $K V_D / \omega_{pe} = 1$

$$K = \frac{\omega_{pe}}{V_D}$$

$$\frac{\partial K}{\partial V_D} = - \frac{\omega_{pe}}{V_D^2}$$

so

$$\frac{\partial^2 \gamma}{\partial V_D^2} = + \frac{\omega_{pe}^2}{V_D^4} \frac{\partial^2 \gamma}{\partial K^2} = - \frac{4 \omega_{pe}}{V_D^2}$$

$$\frac{\partial^2 \gamma}{\partial K^2} = - \frac{4 V_D^2}{\omega_{pe}} \quad . \tag{B5}$$

Using this expression in Eq. B4 gives

$$\delta K = \sqrt{\frac{\omega_{pe}\ \ell n2}{4\ V_D^2\ t}}$$

$$= \frac{\sqrt{\ell n2}}{2V_D}\sqrt{\frac{\omega_{pe}}{t}}$$

$$= \frac{\sqrt{\ell n2}}{2V_D}\sqrt{\frac{\omega_{pe}\gamma_o}{\tau}} \qquad \text{(B6)}$$

where $\tau = \gamma_o t$. Equation 2.3 gives

$$\gamma_o \simeq \frac{\sqrt{3}}{2}\ (m/2M)^{1/3}\ \omega_{pe}\ . \qquad \text{(B7)}$$

Equation B6 then becomes

$$\delta K = \frac{\sqrt{\ell n2}}{2V_D}\ \sqrt{\frac{\sqrt{3}}{2}\ (m/2M)^{1/3}\ \frac{\omega_{pe}^2}{\tau}}\ . \qquad \text{(B8)}$$

For an argon plasma this is

$$\delta K = \frac{\sqrt{\ell n2}}{2V_D}\sqrt{\frac{\sqrt{3}}{2}\left(\frac{1}{2(40)(1836)}\right)^{1/3}\ \frac{\omega_{pe}^2}{\tau}}$$

$$= .053\ \frac{\omega_{pe}}{V_D}\ \frac{1}{\sqrt{\tau}}$$

$$= .053\ \frac{K}{\sqrt{\tau}}\ . \qquad \text{(B9)}$$

Ishihara et al. (1980) predicts saturation of the instability and current beam collapse after about $\tau = 8$. By this time the electric field energy spectrum has compressed to

$$\frac{\delta K}{K} = \frac{.053}{\sqrt{\tau}} \simeq .02 \text{ or } 2\%\ .$$